Available online at www.sciencedirect.com
ScienceDirect
International Journal of Multiphase Flow 33 (2007) 616–637
International Journal of Multiphase Flow
www.elsevier.com/locate/ijmulflow

Assessment of filtered gas–solid momentum transfer models via a linear wave propagation speed test

Juray De Wilde [a,*], Denis Constales [c], Geraldine J. Heynderickx [b], Guy B. Marin [b]

[a] *Materials and Process Engineering Department (IMAP), Université catholique de Louvain, Réaumur, Place Sainte Barbe 2, B-1348 Louvain-la-Neuve, Belgium*
[b] *Laboratorium voor Petrochemische Techniek, Ghent University, Krijgslaan 281, Blok S5, B-9000 Gent, Belgium*
[c] *Department of Applied Mathematics, Ghent University, Galglaan, B-9000 Gent, Belgium*

Received 22 November 2006; received in revised form 14 December 2006

Abstract

The propagation speeds of linear waves in gas–solid suspensions depend strongly on the solids volume fraction and the wave frequency. The latter is due to gas–solid momentum transfer and allows a simple test on filtered gas–solid momentum transfer models. Such models may predict linear wave propagation speeds different from those obtained with the non-filtered model at wave frequencies higher than the filter frequency, but not at wave frequencies lower than the filter frequency.

For the filtered drag, an effective drag coefficient approach is shown to alter the linear wave propagation speeds in the entire wave frequency range, independent of the applied effective drag coefficient. Furthermore, as the effective drag coefficient decreases, the high frequency linear wave propagation speeds are gradually introduced at lower wave frequencies. For the filtered momentum transfer due to the correlation between the solids volume fraction and the gas phase pressure gradient, the behavior of an apparent added mass closure model and an apparent history force closure model are investigated. An apparent added mass introduces the filter frequency linear wave propagation speeds to frequencies higher than the filter frequency. The linear wave propagation speeds for wave frequencies lower than the filter frequency are, however, not altered. Furthermore, an apparent added mass introduces no intrinsic wave frequency dependence in the linear wave propagation speeds, in agreement with its source term in the non-filtered model. Hence, the frequency dependence of the linear wave propagation speeds at frequencies lower than the filter frequency is still to be provided by a drag type term. As such, the behavior introduced by an apparent added mass is acceptable for filtered models. Also, to a certain extent, an apparent added mass can restore the linear wave propagation speed behavior at wave frequencies lower than the filter frequency altered by an effective drag coefficient approach. The reformulation of the apparent added mass in terms of an apparent distribution of the filtered gas phase pressure gradient over the phases and an apparent (effective) drag force is investigated. An apparent history force introduces intrinsic wave frequency dependence in the linear wave propagation speeds and alters the latter from the low wave frequencies on. As such, the behavior introduced by an apparent history force is unacceptable for filtered models.
© 2006 Elsevier Ltd. All rights reserved.

Keywords: Linear wave propagation speed; Mixture speed of sound; Filtering; Gas–solid flow; Modeling; Eigenvalue analysis

* Corresponding author. Tel.: +32 10 47 8193; fax: +32 10 47 4028.
E-mail address: dewilde@imap.ucl.ac.be (J. De Wilde).

0301-9322/$ - see front matter © 2006 Elsevier Ltd. All rights reserved.
doi:10.1016/j.ijmultiphaseflow.2006.12.003

1. Introduction

Eulerian–Eulerian gas–solid flow models describe the gas phase and the solid phase as entirely mixed continua (Anderson and Jackson, 1967). The non-filtered set of partial differential transport equations with source terms covers phenomena over the entire spatial and angular wave frequency range ω but cannot be integrated analytically. A numerical solution of a set of discretized algebraic equations on a spatial and temporal mesh is possible but requires very small and computationally not tractable mesh sizes. To reduce the computational cost, finite size spatial and temporal meshes are used (often macro-scale), introducing a certain filter frequency ω_f (Pope, 2000). The latter can be spatially or temporally determined. Phenomena of a frequency ω higher than the filter frequency ω_f, so-called sub-grid-scale phenomena, are not explicitly calculated and filtered out by the mesh. Phenomena with a frequency ω lower than the filter frequency ω_f are, on the other hand, explicitly calculated. To account for the effects of the sub-grid-scale phenomena, filtered models have to be used (Pope, 2000). Filtered models introduce their own filter frequency ω_f. In general, the filter frequency ω_f is defined as the frequency up to which phenomena can be explicitly and accurately calculated, that is as with a non-filtered approach.

As a result of filtering, extra, correlation terms appear in filtered models (Pope, 2000; Zhang and VanderHeyden, 2002). These correlation terms describe the sub-grid-scale phenomena and create a closure problem, that is they have to be modeled in terms of the filtered variables. Via the closure model approach, phenomena should be described the way they appear (that is, in an apparent way), so to say from a distance. The closure model parameters have to be quantified or modeled based on the underlying physics.

For single phase flows, many different approaches to solve the closure problem have been developed (Pope, 2000). For gas–solid flows, on the other hand, and for multi-phase flows in general, the solution of the closure problem is in the early stage of development (Agrawal et al., 2001; Zhang and VanderHeyden, 2002; Heynderickx et al., 2004; Andrews et al., 2005). Only a few research groups have proposed closure models for some of the correlation terms appearing in filtered gas–solid flow models (Zhang and VanderHeyden, 2002; Yang et al., 2003; Heynderickx et al., 2004; Andrews et al., 2005). Because gas–solid momentum transfer plays a crucial role in the behavior of gas–solid flows, the focus has been on the filtered gas–solid momentum transfer terms so far.

Gas–solid flows exhibit an interesting behavior with respect to wave frequency dependence. The linear wave propagation speeds in gas–solid mixtures, and in particular the so-called mixture speed of sound c_m which dictates the propagation of gas phase pressure waves in gas–solid mixtures and which is derived from the linear wave propagation speeds, strongly depend on the solids volume fraction and, more importantly for the present investigation, on the wave frequency (Atkinson and Kytömaa, 1992; Gregor and Rumpf, 1975, 1976). The complex linear wave propagation speed behavior in gas–solid mixtures is a result of gas–solid momentum transfer. In practical gas–solid flows, a broad range of wave frequencies and solids volume fractions occur. The remarkable difference between the single gas phase speed of sound (c_g, of the order of 330 m/s) and the mixture speed of sound (c_m, down to the order of 10 m/s) on the one hand, and the wave frequency and solids volume fraction dependence of the mixture speed of sound on the other hand, are at the origin of physical and computational complex behavior of gas–solid flows. For example, the extension of preconditioning techniques and certain discretization schemes from single phase flows to gas–solid flows is not straightforward (De Wilde et al., 2002, 2005a,c).

A linear wave propagation analysis was shown to be a powerful tool in evaluating multiphase flow models (Boure, 1997a,b). One of the early successes of the non-filtered Eulerian–Eulerian gas–solid flow model was its capability of describing the complex linear wave propagation speed behavior over the entire solids volume fraction and wave frequency ranges (Gregor and Rumpf, 1975, 1976). The gas–solid drag was found to play a crucial role in the calculated linear wave propagation speed behavior of gas–solid flows. The wave frequency dependence of the linear wave propagation speeds in gas–solid mixtures then suggests an interesting necessary test for filtered gas–solid flow models. Such models should still describe correctly the linear wave propagation speeds for wave frequencies lower than the filter frequency, but not necessarily for wave frequencies higher than the filter frequency. It is the purpose of this paper to investigate the linear wave propagation speed behavior obtained with some filtered gas–solid flow/momentum transfer models presented in the literature and to demonstrate the information that can be obtained from a linear wave propagation speed test. Particular

attention is paid to the wave frequency range influenced by the filtered model closures for gas–solid momentum transfer.

2. Modeling

2.1. Non-filtered model

The basic non-filtered Eulerian–Eulerian model equations describe the conservation of mass and momentum for each phase (Anderson and Jackson, 1967):

Mass conservation solid phase.

$$\frac{\partial}{\partial t}(\varepsilon_s \rho_s) + \frac{\partial}{\partial \mathbf{r}} \cdot (\varepsilon_s \rho_s \mathbf{v}) = 0 \tag{1}$$

Mass conservation gas phase.

$$\frac{\partial}{\partial t}(\varepsilon_g \rho_g) + \frac{\partial}{\partial \mathbf{r}} \cdot (\varepsilon_g \rho_g \mathbf{u}) = 0 \tag{2}$$

Momentum conservation solid phase.

$$\frac{\partial}{\partial t}(\varepsilon_s \rho_s \mathbf{v}) + \frac{\partial}{\partial \mathbf{r}} \cdot (\varepsilon_s \rho_s \mathbf{v}\mathbf{v}) = -\frac{\partial P_s}{\partial \mathbf{r}} - \frac{\partial}{\partial \mathbf{r}} \cdot (\varepsilon_s \boldsymbol{s}_s) + \varepsilon_s \rho_s \mathbf{g} - \varepsilon_s \frac{\partial P}{\partial \mathbf{r}} + \beta(\mathbf{u} - \mathbf{v}) \tag{3}$$

where

$$\boldsymbol{s}_s = -\left[\left(\xi_s - \frac{2}{3}\mu_s\right)\left(\frac{\partial}{\partial \mathbf{r}} \cdot \mathbf{v}\right)\boldsymbol{I} + (\mu_s)\left(\left(\frac{\partial}{\partial \mathbf{r}}\mathbf{v}\right) + \left(\frac{\partial}{\partial \mathbf{r}}\mathbf{v}\right)^T\right)\right] \tag{4}$$

Momentum conservation gas phase.

$$\frac{\partial}{\partial t}(\varepsilon_g \rho_g \mathbf{u}) + \frac{\partial}{\partial \mathbf{r}} \cdot (\varepsilon_g \rho_g \mathbf{u}\mathbf{u}) = -\frac{\partial P}{\partial \mathbf{r}} - \frac{\partial}{\partial \mathbf{r}} \cdot \boldsymbol{s}_g + \varepsilon_g \rho_g \mathbf{g} + \varepsilon_s \frac{\partial P}{\partial \mathbf{r}} - \beta(\mathbf{u} - \mathbf{v}) \tag{5}$$

where

$$\boldsymbol{s}_g = -\left[\left(\xi_g - \frac{2}{3}\mu_g\right)\left(\frac{\partial}{\partial \mathbf{r}} \cdot \mathbf{u}\right)\boldsymbol{I} + (\mu_g)\left(\left(\frac{\partial}{\partial \mathbf{r}}\mathbf{u}\right) + \left(\frac{\partial}{\partial \mathbf{r}}\mathbf{u}\right)^T\right)\right] \tag{6}$$

in which ε_s and ε_g are respectively the solid phase and the gas phase volume fraction. Bold and bold italic character types are used for vectors and tensors, respectively.

Analogous to the gas phase pressure P and the gas phase shear stress $\boldsymbol{s}_g$, a solid phase pressure P_s and solid phase shear stress $\boldsymbol{s}_s$ are introduced (Eqs. (3) and (4)). The latter can be calculated via empirical correlations or via the Kinetic Theory of Granular Flow (KTGF) (Jenkins and Savage, 1983; Gidaspow, 1994), requiring the integration of an additional granular temperature transport equation.

The last two (source) terms in Eqs. (3) and (5) describe the gas–solid momentum transfer. The latter consists of the solids volume fraction of the gas phase pressure gradient $-\varepsilon_s \frac{\partial P}{\partial \mathbf{r}}$ and of the drag force $\beta(\mathbf{u} - \mathbf{v})$, corresponding to model A as defined by Gidaspow (1994). Most commonly, the Ergun equation (Ergun, 1952) and the equation of Wen and Yu (1966) are used for the calculation of the drag coefficient β. For the constitutive equations, reference is made to De Wilde et al. (2002). Due to the large density differ-

ence between gas and solids, other interphase forces, as for example the added mass and Basset history forces, are usually neglected in the non-filtered gas–solid flow model.

2.2. Filtered models

Starting from the non-filtered model (Eqs. (1)–(6)), a filtered model is obtained by formally Reynolds–Favre-like-averaging (Pope, 2000; Zhang and VanderHeyden, 2002). For the solids volume fraction ε_s and the gas phase pressure P, Reynolds-averaging $\langle\ \rangle$ is applied. Assuming a statistical steady state over a time period Δt_f used for averaging i.e. the inverse of the filter frequency ω_f, the filtered solids volume fraction $\langle\varepsilon_s\rangle$ and the filtered gas phase pressure $\langle P\rangle$ are defined as

$$\langle\varepsilon_s\rangle = \frac{1}{\Delta t_f}\int_t^{t+\Delta t_f} \varepsilon_s(t)\,\mathrm{d}t \tag{7}$$

respectively

$$\langle P\rangle = \frac{1}{\Delta t_f}\int_t^{t+\Delta t_f} P(t)\,\mathrm{d}t \tag{8}$$

An instantaneous value can be written in terms of its Reynolds-averaged value and a fluctuation:

$$\varepsilon_s = \langle\varepsilon_s\rangle + \varepsilon_s' \tag{9}$$

$$P = \langle P\rangle + P' \tag{10}$$

It can be shown that

$$\langle\varepsilon_s'\rangle = 0 \quad \text{and} \quad \langle P'\rangle = 0 \tag{11}$$

For variables ϕ, other than the gas phase pressure and the solids volume fraction, Favre-like-averaging $\{\ \}$ is applied using respectively the solids volume fraction for the solid phase variables and the gas phase volume fraction for the gas phase variables. For example, for a solid phase variable ϕ:

$$\{\phi\} = \frac{\frac{1}{\Delta t_f}\int_t^{t+\Delta t_f} \varepsilon_s(t)\phi(t)\,\mathrm{d}t}{\frac{1}{\Delta t_f}\int_t^{t+\Delta t_f} \varepsilon_s(t)\,\mathrm{d}t} = \frac{\langle\varepsilon_s\phi\rangle}{\langle\varepsilon_s\rangle} \tag{12}$$

An instantaneous value can be written in terms of its Favre-like-averaged value and a fluctuation:

$$\phi = \{\phi\} + \phi' \tag{13}$$

In this case:

$$\{\phi'\} \neq 0 \tag{14}$$

Neglecting sub-grid-scale fluctuations in the gas phase density ρ_g' and introducing Eqs. (9), (10) and (13) in Eqs. (1)–(3) and (5), the following filtered gas–solid flow model is obtained:

Filtered mass conservation solid phase:

$$\frac{\partial}{\partial t}(\langle\varepsilon_s\rangle\rho_s) + \frac{\partial}{\partial \mathbf{r}}\cdot(\langle\varepsilon_s\rangle\rho_s\{\mathbf{v}\}) = 0 \tag{15}$$

Filtered mass conservation gas phase:

$$\frac{\partial}{\partial t}(\langle\varepsilon_g\rangle\rho_g) + \frac{\partial}{\partial \mathbf{r}}\cdot(\langle\varepsilon_g\rangle\rho_g\{\mathbf{u}\}) = 0 \tag{16}$$

Filtered momentum conservation solid phase:

$$\frac{\partial}{\partial t}(\langle\varepsilon_s\rangle\rho_s\{\mathbf{v}\}) + \frac{\partial}{\partial \mathbf{r}}\cdot(\langle\varepsilon_s\rangle\rho_s\{\mathbf{v}\}\{\mathbf{v}\}) = -\frac{\partial}{\partial \mathbf{r}}\langle P_s\rangle - \frac{\partial}{\partial \mathbf{r}}\cdot(\langle\varepsilon_s\rangle\{\tilde{\mathbf{s}}_s\}) + \langle\varepsilon_s\rangle\rho_s\mathbf{g} - \left\langle\varepsilon_s\frac{\partial P}{\partial \mathbf{r}}\right\rangle + \langle\beta(\mathbf{u}-\mathbf{v})\rangle \tag{17}$$

Filtered momentum conservation gas phase:

$$\frac{\partial}{\partial t}(\langle\varepsilon_g\rangle\rho_g\{\mathbf{u}\}) + \frac{\partial}{\partial \mathbf{r}}\cdot(\langle\varepsilon_g\rangle\rho_g\{\mathbf{u}\}\{\mathbf{u}\}) = -\frac{\partial\langle P\rangle}{\partial \mathbf{r}} - \frac{\partial}{\partial \mathbf{r}}\cdot\langle\tilde{\mathbf{s}}_g\rangle + \langle\varepsilon_g\rangle\rho_g\mathbf{g} + \left\langle\varepsilon_s\frac{\partial P}{\partial \mathbf{r}}\right\rangle - \langle\beta(\mathbf{u}-\mathbf{v})\rangle \tag{18}$$

Currently, no reliable closure models are available for the convection related correlation terms in the filtered gas/solid momentum equations (involving $\langle u'u'\rangle, \langle v'v'\rangle, \langle\varepsilon_g'u'\rangle, \langle\varepsilon_s'v'\rangle, \ldots$ -type correlations). These terms are, however, of minor importance for the present work. Commonly, they are incorporated in the viscous shear terms (Eqs. (17) and (18)). In what follows, the focus is on the closure models for the filtered gas–solid momentum transfer terms, the last two terms on the right hand side of Eqs. (17) and (18). The filtered gas–solid momentum transfer term $\langle\varepsilon_s\frac{\partial P}{\partial \mathbf{r}}\rangle$ can be easily decomposed, introducing the correlation between the solids volume fraction and the gas phase pressure gradient $\langle\varepsilon_s'\frac{\partial P'}{\partial \mathbf{r}}\rangle$:

$$\left\langle\varepsilon_s\frac{\partial P}{\partial \mathbf{r}}\right\rangle = \langle\varepsilon_s\rangle\left\langle\frac{\partial P}{\partial \mathbf{r}}\right\rangle + \left\langle\varepsilon_s'\frac{\partial P'}{\partial \mathbf{r}}\right\rangle \tag{19}$$

2.2.1. Closure models for the filtered drag force

Recent studies by Agrawal et al. (2001) and Zhang and VanderHeyden (2002) have shown a significant reduction of the drag coefficient by the presence of solid phase mesoscale structures (clusters). To account for the latter in coarse mesh simulations in which the solid phase mesoscale structures are filtered out, Yang et al. (2003), Heynderickx et al. (2004) and Andrews et al. (2005) have introduced a filtered or effective drag coefficient β_e, closing the filtered drag force:

$$\langle\beta(\mathbf{u}-\mathbf{v})\rangle = \beta_e(\{\mathbf{u}\}-\{\mathbf{v}\}) \tag{20}$$

The filter frequency is not explicitly accounted for in the effective drag coefficient formulations derived by Yang et al. (2003) and Heynderickx et al. (2004). Andrews et al. (2005) investigated both the time-averaged β_e approach (Eq. (20)) and a stochastic correction. Both the formulations of Yang et al. (2003) and Heynderickx et al. (2004) predict a reduction of the drag coefficient by a factor 1.5–4, depending on the filtered solids volume fraction, in agreement with the reduction calculated from dynamic mesoscale simulations on a periodic $2\times 8\ \mathrm{cm}^2$ domain by Agrawal et al. (2001). With respect to the latter simulations, it should, however, be remarked that the ratio of the domain size used for averaging or filtering and the mesh size is only 32, i.e. only a limited amount of effects is filtered out. Hence, it is possible that for lower filter frequencies ω_f, e.g. in case of steady-state simulations, as more effects are filtered out, the value of the effective drag coefficient is further reduced. The latter is in particular the case if the apparent or generalized added mass (Zhang and VanderHeyden, 2002; De Wilde, 2005b) becomes large, which is possible at low filter frequencies ω_f. This is discussed further in this paper.

In the present work, the effective drag coefficient formulation of Heynderickx et al. (2004) and the drag coefficient of Wen and Yu (1966) reduced with a constant factor, are used to investigate the effect of a reduced drag coefficient approach on the linear wave propagation speed behavior of filtered gas–solid flow models.

2.2.2. Closure models for the correlation between the solids volume fraction and the gas phase pressure gradient

Zhang and VanderHeyden (2002) were the first to study the correlation between the solids volume fraction and the gas phase pressure gradient $\langle\varepsilon_s'\frac{\partial P'}{\partial \mathbf{r}}\rangle$ (Eq. (19)) and found it to be surprisingly important. These authors propose to model $\langle\varepsilon_s'\frac{\partial P'}{\partial \mathbf{r}}\rangle$ via a generalized or apparent added mass term:

$$\left\langle \varepsilon_s' \frac{\partial P'}{\partial \mathbf{r}} \right\rangle = C_a \langle \rho_m \rangle \left(\frac{\partial \{\mathbf{v}\}}{\partial t} + \{\mathbf{v}\} \cdot \frac{\partial \{\mathbf{v}\}}{\partial \mathbf{r}} - \frac{\partial \{\mathbf{u}\}}{\partial t} - \{\mathbf{u}\} \cdot \frac{\partial \{\mathbf{u}\}}{\partial \mathbf{r}} \right) \tag{21}$$

which scales with the volume fraction based mixture density ρ_m and the apparent added mass coefficient C_a for which a formulation as a function of the filter frequency ω_f is yet to be derived. As the filter frequency ω_f goes to infinity (towards non-filtered), the correlation terms and, hence, the apparent added mass (coefficient) must vanish. De Wilde (2005b) showed that an apparent added mass contribution from $\langle \varepsilon_s' \frac{\partial P'}{\partial \mathbf{r}} \rangle$ is partially direct and partially indirect and that the direct contribution scales according to the mean square of the solids volume fraction fluctuations $\langle \varepsilon_s' \varepsilon_s' \rangle$. Furthermore, the direct contribution to the apparent added mass was shown to account for about 90% of $\langle \varepsilon_s' \frac{\partial P'}{\partial \mathbf{r}} \rangle$. According to Zhang and VanderHeyden (2002) and De Wilde (2005b), C_a can be much larger than one, resulting in an apparent added mass that is much larger than the well-known added mass (Crowe et al., 1997; Ranade, 2002).

De Wilde (2005b) showed that the introduction of an apparent added mass amounts to a redistribution of the filtered gas phase pressure gradient over the phases. This makes the apparent added mass more comprehensible. The presence of the drag force was, however, neglected in the analysis. A more complete reformulation and interpretation of the apparent added mass will be discussed further in this paper.

To illustrate the linear wave propagation speed test, an apparent (or generalized) history force closure model approach for the correlation between the solids volume fraction and the gas phase pressure gradient $\langle \varepsilon_s' \frac{\partial P'}{\partial \mathbf{r}} \rangle$ is investigated as well:

$$\left\langle \varepsilon_s' \frac{\partial P'}{\partial \mathbf{r}} \right\rangle = C_h \langle \rho_m \rangle \int_0^t \frac{\frac{\partial \{\mathbf{v}\}}{\partial t'} + \{\mathbf{v}\} \cdot \frac{\partial \{\mathbf{v}\}}{\partial \mathbf{r}} - \frac{\partial \{\mathbf{u}\}}{\partial t'} - \{\mathbf{u}\} \cdot \frac{\partial \{\mathbf{u}\}}{\partial \mathbf{r}}}{\sqrt{t - t'}} \, dt' \tag{22}$$

with C_h the apparent history force coefficient.

With respect to the apparent history force, it should be stressed that there is no evidence so far for its appearance or importance. In this early stage of the development of filtered gas–solid flow models, however, it is unclear what type of description is to be used to describe gas–solid momentum transfer in a filtered way. Nevertheless, it should be emphasized that it is not the aim of the present paper to develop or propose new closures for the filtered gas–solid momentum transfer, but to present and illustrate a test for such closures. Hence, in what follows, the apparent history force is mainly investigated to illustrate this test.

Remark that in the well-known Basset history force (Basset, 1961; Mei, 1993), the integral over time is premultiplied with the square root of the gas phase density. It is, however, assumed that the apparent history force (Eq. (22)) scales with the mixture density, analogous to the apparent added mass (Eq. (21)). Furthermore, the kernel in Eq. (22) has been originally derived for spherical, non-deformable objects at low Reynolds numbers and for small time scales. For non-spherical or deformable objects, as for example solids clusters, the kernel is in fact not as simple. Also, for larger time scales, the relation with the inverse square root of the time in Eq. (22) can be questioned.

Nevertheless, a possible way to picture the apparent history force is in analogy to the Basset history force, i.e. resulting from the gas–solids mixture wakes behind solids clusters. The viscosity in a gas–solids wake is expected to be several orders of magnitude higher than the single gas phase viscosity, which could justify the appearance of an apparent history force. As such, the apparent history force coefficient C_h could depend on the inverse of the square root of the time scale of the solids clusters. If the time scale of the solids clusters goes to infinity, the solids structures are not filtered out and C_h goes to zero as it should.

As the filter frequency ω_f decreases, the correlation between the solids volume fraction and the gas phase pressure gradient $\langle \varepsilon_s' \frac{\partial P'}{\partial \mathbf{r}} \rangle$ grows in importance and the value of the apparent added mass coefficient C_a (Eq. (21)) or the apparent history force coefficient C_h (Eq. (22)) is expected to increase.

3. Analysis of the linear wave propagation speeds

To correctly calculate gas–solid flows, it is important that the linear wave propagation speeds obtained from the gas–solid flow model correspond to the physically observed linear wave propagation speeds.

A linear wave propagation speed analysis is performed on the one-dimensional solid phase and gas phase mass and momentum conservation equations and assuming a uniform steady-state flow field. Remark that

viscous terms, neglected in a 1D analysis, hardly alter the linear wave propagation speeds of the gas–solid flow system, in contrast to source terms (Arai, 1980; Ransom and Hicks, 1984; Stewart and Wendroff, 1984; Prosperetti and Jones, 1987; Ransom and Hicks, 1988). This justifies the use of an inviscid model for the determination of the linear wave propagation speeds.

3.1. Non-filtered model

The set of partial differential equations, Eqs. (1)–(3) and (5), expressing the conservation of mass and momentum for each phase, is written in matrix formulation:

$$\frac{\partial \mathbf{Q}}{\partial t}+\frac{\partial \mathbf{F}}{\partial x}=\mathbf{K} \tag{23}$$

where $\mathbf{Q}$ is the (4×1) matrix of the conservative variables (i.e. mass and momentum in each of the phases $\varepsilon_s\rho_s$, $\varepsilon_g\rho_g$, $\varepsilon_s\rho_s v$, $\varepsilon_g\rho_g u$), $\mathbf{F}$ includes both the convective fluxes and the gas and solid phase pressure gradients $\partial P/\partial x$ and $\partial P_s/\partial x$, and $\mathbf{K}$ contains the gravity and the gas–solid momentum transfer source terms, i.e. the drag force $\pm\beta(u-v)$ and the solids volume fraction of the gas phase pressure gradient $\mp\varepsilon_s\,\partial P/\partial x$.

Sinusoidal perturbations will be imposed to calculate the linear wave propagation speeds. For a perturbation $\delta\mathbf{Q}$, Eq. (23) transforms into:

$$\frac{\partial(\delta\mathbf{Q})}{\partial t}+\frac{\partial(\delta\mathbf{F})}{\partial x}=(\delta\mathbf{K}) \tag{24}$$

To obtain the linear wave propagation speeds, the time derivative term, the flux terms and the source terms in equation set Eq. (24) are linearized in terms of the primitive variables $\mathbf{X}$ (i.e. ε_s, P, v, and u):

$$\frac{\partial \boldsymbol{Q}}{\partial \boldsymbol{X}}\cdot\frac{\partial(\delta\mathbf{X})}{\partial t}+\frac{\partial \boldsymbol{F}}{\partial \boldsymbol{X}}\cdot\frac{\partial(\delta\mathbf{X})}{\partial x}=\frac{\partial \boldsymbol{K}}{\partial \boldsymbol{X}}\cdot(\delta\mathbf{X}) \tag{25}$$

introducing the Jacobian:

$$\frac{\partial \boldsymbol{Q}}{\partial \boldsymbol{X}}=\begin{pmatrix}\rho_s & 0 & 0 & 0\\ -\rho_g & \varepsilon_g\rho_g/P & 0 & 0\\ \rho_s v & 0 & \varepsilon_s\rho_s & 0\\ -\rho_g u & \varepsilon_g u\rho_g/P & 0 & \varepsilon_g\rho_g\end{pmatrix} \tag{26}$$

while

$$\frac{\partial \boldsymbol{F}}{\partial \boldsymbol{X}}=\begin{pmatrix}\rho_s v & 0 & \varepsilon_s\rho_s & 0\\ -\rho_g u & \varepsilon_g u\rho_g/P & 0 & \varepsilon_g\rho_g\\ M+\rho_s vv & \varepsilon_s & 2\varepsilon_s\rho_s v & 0\\ -\rho_g uu & \varepsilon_g+\varepsilon_g uu\rho_g/P & 0 & 2\varepsilon_g\rho_g u\end{pmatrix} \tag{27}$$

with the solids stress modulus M (Gidaspow, 1994):

$$M=\frac{\partial P_s}{\partial \varepsilon_s} \tag{28}$$

The ideal gas law is assumed when accounting for the compressibility of the gas phase, i.e. $\frac{\partial\rho_g}{\partial P}=\frac{\rho_g}{P}$.

The Jacobian of the gravity and drag source terms $\partial \boldsymbol{K}/\partial \boldsymbol{X}$ is given by:

$$\frac{\partial \boldsymbol{K}}{\partial \boldsymbol{X}}=\begin{pmatrix}0 & 0 & 0 & 0\\ 0 & 0 & 0 & 0\\ \rho_s g+\frac{\partial I_{gs}^{drag}}{\partial \varepsilon_s} & \frac{\partial I_{gs}^{drag}}{\partial P} & \frac{\partial I_{gs}^{drag}}{\partial v} & \frac{\partial I_{gs}^{drag}}{\partial u}\\ -\rho_g g-\frac{\partial I_{gs}^{drag}}{\partial \varepsilon_s} & \frac{\varepsilon_g\rho_g g}{P}-\frac{\partial I_{gs}^{drag}}{\partial P} & -\frac{\partial I_{gs}^{drag}}{\partial v} & -\frac{\partial I_{gs}^{drag}}{\partial u}\end{pmatrix} \tag{29}$$

with: $\Gamma_{gs}^{drag} = \beta(u - v)$. The partial derivatives in Eq. (29) can be calculated analytically or numerically, e.g.

$$\frac{\partial \Gamma_{gs}^{drag}}{\partial \varepsilon_s} = \frac{\Gamma_{gs}^{drag}(\varepsilon_s + \Delta\varepsilon_s) - \Gamma_{gs}^{drag}(\varepsilon_s - \Delta\varepsilon_s)}{2\Delta\varepsilon_s} \tag{30}$$

Introducing:

$$\boldsymbol{A} = \left(\frac{\partial \boldsymbol{Q}}{\partial \boldsymbol{X}}\right)^{-1} \cdot \frac{\partial \boldsymbol{F}}{\partial \boldsymbol{X}} \tag{31}$$

and

$$\boldsymbol{B} = \left(\frac{\partial \boldsymbol{Q}}{\partial \boldsymbol{X}}\right)^{-1} \cdot \frac{\partial \boldsymbol{K}}{\partial \boldsymbol{X}} \tag{32}$$

Eq. (25) can be rewritten as

$$\frac{\partial(\delta \mathbf{X})}{\partial t} + \boldsymbol{A}\frac{\partial(\delta \mathbf{X})}{\partial x} - \boldsymbol{B}(\delta \mathbf{X}) = 0 \tag{33}$$

Performing a Fourier transform (Bracewell, 1965), imposing sinusoidal perturbations with amplitude $\widehat{\mathbf{A}}$, angular wave frequency ω and linear wave propagation speed s:

$$\delta \mathbf{X} = \widehat{\mathbf{A}} e^{i((\omega/s)x - \omega t)} \tag{34}$$

Eq. (25) transforms into:

$$\left(-i\omega \boldsymbol{I} + i\frac{\omega}{s}\boldsymbol{A} - \boldsymbol{B}\right)\delta \mathbf{X} = 0 \tag{35}$$

The amplitude of the perturbations $\widehat{\mathbf{A}}$ differs from zero. Hence, a solution of Eq. (35) requires:

$$\det\left(-i\omega \boldsymbol{I} + i\frac{\omega}{s}\boldsymbol{A} - \boldsymbol{B}\right) = 0 \tag{36}$$

or

$$\det\left(\frac{i\omega}{s}\boldsymbol{I} - i\omega \boldsymbol{A}^{-1} - \boldsymbol{A}^{-1}\boldsymbol{B}\right) = 0 \tag{37}$$

A solution of Eq. (37) requires that:

$$\frac{1}{s} = \frac{1}{i\omega}\text{eigenvalues}(i\omega \boldsymbol{A}^{-1} + \boldsymbol{A}^{-1}\boldsymbol{B}) \tag{38}$$

from which the linear wave propagation speeds s corresponding to a fixed angular wave frequency ω can be solved.

Eq. (38) allows roughly evaluating the impact and the frequency range affected by different closure model types for gas–solid momentum transfer. A drag force type description, independent of ω (as seen from $\boldsymbol{B}$, Eqs. (29) and (32)), will have a big effect over the entire frequency range, due to the division by ω in Eq. (38). A history force type description, proportional to $\sqrt{\omega}$, will have somewhat less effect, whereas an added mass type description, proportional to ω, will have the least effect. The above will be demonstrated further in this paper.

Because an analytical expression for the linear wave propagation speeds cannot always be found, the linear wave propagation speeds are investigated numerically. The linear wave propagation speed analysis was carried out using MAPLE. Two of the four linear wave propagation speeds obtained from Eq. (38) are found to be related to the propagation of the gas phase variables, whereas the two others are found to be related to the propagation of the solid phase variables. Furthermore, in accordance with Gregor and Rumpf (1975, 1976) and Gidaspow (1994), the linear wave propagation speeds can be decomposed as

$$\begin{aligned}[Re(1/s_{1,2})]^{-1} &= \hat{u} \pm c_m(\omega, \varepsilon_s, \rho_s, \rho_g)\\ [Re(1/s_{3,4})]^{-1} &= \hat{v} \pm c_s(M, \rho_s)\end{aligned} \tag{39}$$

where c_m is the mixture speed of sound (Gregor and Rumpf, 1975, 1976; Atkinson and Kytömaa, 1992) and c_s is the so-called granular speed of sound (Gidaspow, 1994), related to the propagation of the solid phase pressure P_s. Hence, the mixture speed of sound c_m is calculated from:

$$c_m = \frac{\left(\left[Re\left(\frac{1}{s_1}\right)\right]^{-1} - \left[Re\left(\frac{1}{s_2}\right)\right]^{-1}\right)}{2} \tag{40}$$

The analysis of the linear wave propagation speeds showed that the mixture speed of sound c_m is not influenced by the granular speed of sound c_s.

3.2. Filtered models

The analysis of the linear wave propagation speeds of filtered models is analogous to the analysis of the linear wave propagation speeds of the non-filtered model but filtered variables $\langle\ \rangle$ (Eqs. (7) and (8)) and $\{\ \}$ (Eq. (12)) are involved and extra terms appear in the equations, depending on the closure models that are used for the filtered gas–solid momentum transfer terms.

3.2.1. Effective drag coefficient approach for the filtered drag force

Applying the effective drag coefficient approach for the filtered drag force (Eq. (20)) (e.g. Heynderickx et al., 2004), the constitutive equation for the drag coefficient is modified in the linear wave propagation speed analysis.

3.2.2. Apparent added mass approach for the correlation between the solids volume fraction and the gas phase pressure gradient

The Fourier transform of an apparent added mass term (Eq. (21)) is straightforward. The Jacobians $\left\langle\frac{\partial \boldsymbol{Q}}{\partial \boldsymbol{X}}\right\}$ and $\left\langle\frac{\partial \boldsymbol{F}}{\partial \boldsymbol{X}}\right\}$ in filtered Eq. (25) become:

$$\frac{\partial\langle \boldsymbol{Q}\}}{\partial\langle \boldsymbol{X}\}} = \begin{pmatrix} \rho_s & 0 & 0 & 0 \\ -\rho_g & \langle\varepsilon_g\rangle\rho_g/\langle P\rangle & 0 & 0 \\ \rho_s\{v\} & 0 & \langle\varepsilon_s\rangle\rho_s + C_a\langle\rho_m\rangle & -C_a\langle\rho_m\rangle \\ -\rho_g\{u\} & \langle\varepsilon_g\rangle\{u\}\rho_g/\langle P\rangle & -C_a\langle\rho_m\rangle & \langle\varepsilon_g\rangle\rho_g + C_a\langle\rho_m\rangle \end{pmatrix} \tag{41}$$

and

$$\frac{\partial\langle \boldsymbol{F}\}}{\partial\langle \boldsymbol{X}\}} = \begin{pmatrix} \rho_s\{v\} & 0 & \langle\varepsilon_s\rangle\rho_s & 0 \\ -\rho_g\{u\} & \langle\varepsilon_g\rangle\{u\}\rho_g/\langle P\rangle & 0 & \langle\varepsilon_g\rangle\rho_g \\ M + \rho_s\{v\}\{v\} & \langle\varepsilon_s\rangle & 2\langle\varepsilon_s\rangle\rho_s\{v\} + C_a\langle\rho_m\rangle\{v\} & -C_a\langle\rho_m\rangle\{u\} \\ -\rho_g\{u\}\{u\} & \langle\varepsilon_g\rangle + \langle\varepsilon_g\rangle\{u\}\{u\}\rho_g/\langle P\rangle & -C_a\langle\rho_m\rangle\{v\} & 2\langle\varepsilon_g\rangle\rho_g\{u\} + C_a\langle\rho_m\rangle\{u\} \end{pmatrix} \tag{42}$$

3.2.3. Apparent history force approach for the correlation between the solids volume fraction and the gas phase pressure gradient

The Fourier transform of an apparent history force (Eq. (22)) is obtained using the convolution theorem (Bracewell, 1965):

$$\begin{aligned} &\mathfrak{I}_t\,\mathfrak{I}_x\left[C_h\langle\rho_m\rangle\int_0^t \frac{\frac{\partial\{v\}}{\partial t'} + \{v\}\cdot\frac{\partial\{v\}}{\partial x} - \frac{\partial\{u\}}{\partial t'} - \{u\}\cdot\frac{\partial\{u\}}{\partial x}}{\sqrt{t-t'}}\,dt'\right] \\ &\quad = C_h\langle\rho_m\rangle\left[\frac{1-i}{\sqrt{\omega}}\sqrt{\frac{\pi}{2}}\right]\mathfrak{I}_t\,\mathfrak{I}_x\left[\frac{\partial\{v\}}{\partial t} + \{v\}\cdot\frac{\partial\{v\}}{\partial x} - \frac{\partial\{u\}}{\partial t} - \{u\}\cdot\frac{\partial\{u\}}{\partial x}\right] \end{aligned} \tag{43}$$

Substituting Eq. (34), Eq. (43) results into:

$$C_h\langle\rho_m\rangle\left[\frac{1-i}{\sqrt{\omega}}\sqrt{\frac{\pi}{2}}\right]\left[-i\omega\delta\{v\}+\{v\}\frac{i\omega}{s}\delta\{v\}+i\omega\delta\{u\}-\{u\}\frac{i\omega}{s}\delta\{u\}\right] \tag{44}$$

which can be added to Eqs. (35), corresponding to the following Jacobians $\left[\frac{\partial\boldsymbol{Q}}{\partial\boldsymbol{X}}\right]$ and $\left[\frac{\partial\boldsymbol{F}}{\partial\boldsymbol{X}}\right]$ in filtered Eq. (25):

$$\frac{\partial[\boldsymbol{Q}]}{\partial[\boldsymbol{X}]}=\begin{pmatrix}\rho_s & 0 & 0 & 0\\ -\rho_g & \langle\varepsilon_g\rangle\rho_g/\langle P\rangle & 0 & 0\\ \rho_s\{v\} & 0 & \langle\varepsilon_s\rangle\rho_s+C_h\langle\rho_m\rangle\left[\frac{1-i}{\sqrt{\omega}}\sqrt{\frac{\pi}{2}}\right] & -C_h\langle\rho_m\rangle\left[\frac{1-i}{\sqrt{\omega}}\sqrt{\frac{\pi}{2}}\right]\\ -\rho_g\{u\} & \langle\varepsilon_g\rangle\{u\}\rho_g/\langle P\rangle & -C_h\langle\rho_m\rangle\left[\frac{1-i}{\sqrt{\omega}}\sqrt{\frac{\pi}{2}}\right] & \langle\varepsilon_g\rangle\rho_g+C_h\langle\rho_m\rangle\left[\frac{1-i}{\sqrt{\omega}}\sqrt{\frac{\pi}{2}}\right]\end{pmatrix} \tag{45}$$

and

$$\frac{\partial[\boldsymbol{F}]}{\partial[\boldsymbol{X}]}=\begin{bmatrix}\rho_s\{v\} & 0 & \langle\varepsilon_s\rangle\rho_s & 0\\ -\rho_g\{u\} & \langle\varepsilon_g\rangle\{u\}\rho_g/\langle P\rangle & 0 & \langle\varepsilon_g\rangle\rho_g\\ M+\rho_s\{v\}\{v\} & \langle\varepsilon_s\rangle & 2\langle\varepsilon_s\rangle\rho_s\{v\}+C_h\langle\rho_m\rangle\left[\frac{1-i}{\sqrt{\omega}}\sqrt{\frac{\pi}{2}}\right]\{v\} & -C_h\langle\rho_m\rangle\left[\frac{1-i}{\sqrt{\omega}}\sqrt{\frac{\pi}{2}}\right]\{u\}\\ -\rho_g\{u\}\{u\} & \langle\varepsilon_g\rangle+\langle\varepsilon_g\rangle\{u\}\{u\}\rho_g/\langle P\rangle & -C_h\langle\rho_m\rangle\left[\frac{1-i}{\sqrt{\omega}}\sqrt{\frac{\pi}{2}}\right]\{v\} & 2\langle\varepsilon_g\rangle\rho_g\{u\}+C_h\langle\rho_m\rangle\left[\frac{1-i}{\sqrt{\omega}}\sqrt{\frac{\pi}{2}}\right]\{u\}\end{bmatrix} \tag{46}$$

4. Results and discussion

4.1. Non-filtered model

Fig. 1 shows the mixture speed of sound $c_m(\omega, \varepsilon_s)$ (Eqs. (38)–(40)) (Gregor and Rumpf, 1975, 1976; Atkinson and Kytömaa, 1992) as a function of the solids volume fraction ε_s and the wave frequency ω calculated via a linear wave propagation speed analysis of the non-filtered model (Eqs. (1)–(6)). It was one of the early successes of the Eulerian–Eulerian gas–solid flow models that the calculated behavior is in agreement with the experimentally observed behavior (Atkinson and Kytömaa, 1992; Gregor and Rumpf, 1975, 1976; van der Schaaf et al., 1998). Higher frequency pressure waves, typically with a frequency higher than 10^6 Hz, propagate quasi-undisturbed through the gas–solid mixture, i.e. the high frequency mixture speed of sound $c_m(\omega, \varepsilon_s)$ equals the single gas phase speed of sound c_g. As the wave frequency ω decreases, the mixture speed of sound $c_m(\omega, \varepsilon_s)$ is gradually decreased by the presence of solid particles. A low wave frequency limit mixture speed of

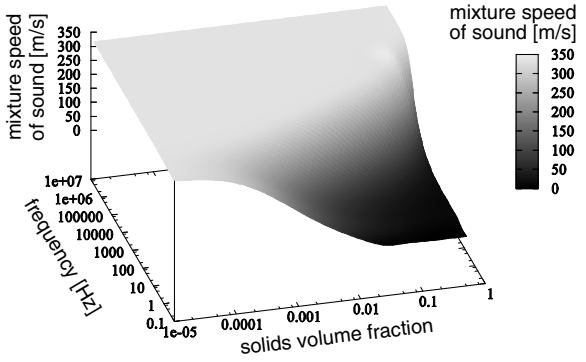

Fig. 1. Mixture speed of sound c_m (Eqs. (38)–(40)) as a function of the angular wave frequency and the solids volume fraction calculated from a linear wave propagation speed analysis of the non-filtered model (Eqs. (1)–(6)). Conditions: $\rho_s = 2650$ kg m^{-3}, $\rho_g = 0.934$ kg m^{-3}, $d_p = 310$ μm and $\langle P\rangle = 104{,}800$ Pa.

sound behavior is observed for wave frequencies ω below 0.1 Hz. At such low wave frequencies, the mixture speed of sound $c_m(\omega, \varepsilon_s)$ gradually decreases from the single gas phase speed of sound c_g for solids volume fractions ε_s lower than 10^{-5} to a minimum mixture speed of sound $c_m(\omega, \varepsilon_s)$ for solids volume fractions ε_s higher than about 0.1. Fig. 2 quantitatively compares the low frequency limit mixture speed of sound c_m (Eqs. (38)–(40)) calculated from the non-filtered model (Eqs. (1)–(6)) and different filtered models (Eqs. (15)–(18)) (discussed later) with experimentally measured values (van der Schaaf et al., 1998). As previously shown by Gregor and Rumpf (1975, 1976); Atkinson and Kytömaa (1992) and others, the non-filtered model describes the experimentally observed mixture speed of sound behavior well.

It should be emphasized that the complex mixture speed of sound behavior calculated (Fig. 1) can be entirely attributed to gas–solid momentum transfer described by the drag force. If the drag force is neglected in the analysis of the linear wave propagation speeds, the mixture speed of sound c_m (Eqs. (38)–(40)) equals the single gas phase speed of sound c_g, independent of the solids volume fraction ε_s and the wave frequency ω.

In the next paragraphs, the mixture speed of sound behavior obtained from different filtered models is compared with the mixture speed of sound behavior obtained from the non-filtered model (Fig. 1).

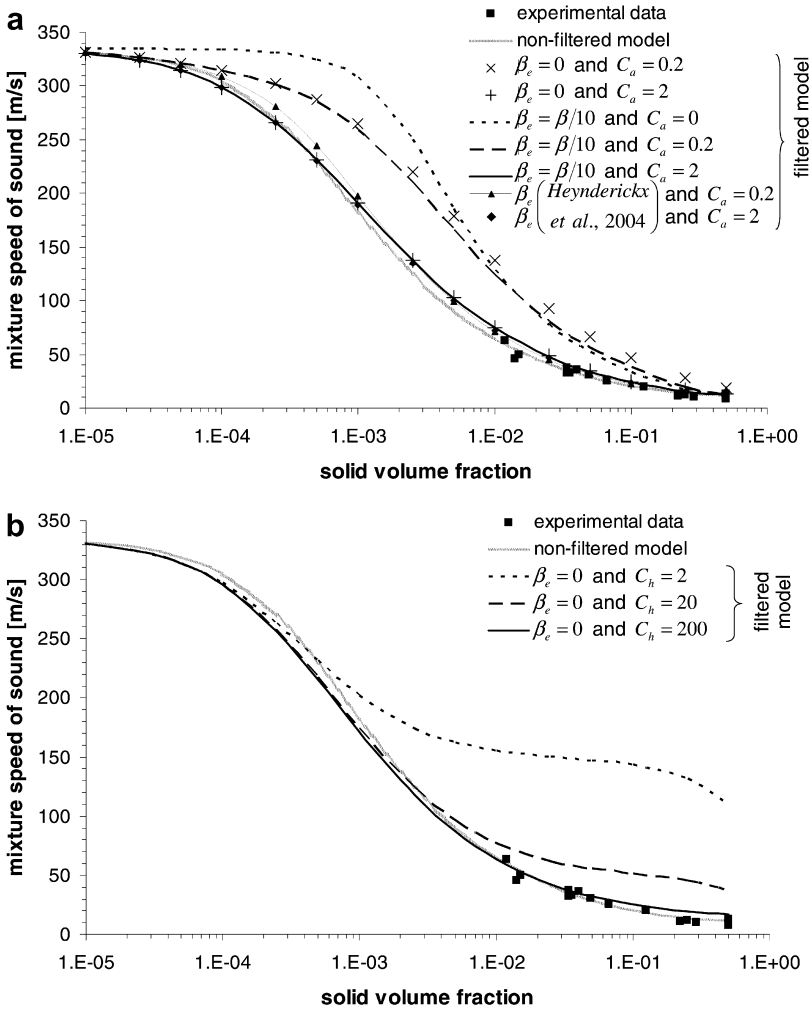

Fig. 2. Comparison of the low-frequency mixture speed of sound c_m (Eqs. (38)–(40)) as a function of the solids volume fraction calculated from a linear wave propagation speed analysis of the non-filtered model A (Eqs. (1)–(6)) and with different filtered models (Eqs. (15)–(22)) with experimentally measured values. Conditions: $\rho_s = 2650\ \mathrm{kg\ m^{-3}}$, $\rho_g = 0.934\ \mathrm{kg\ m^{-3}}$, $d_p = 310\ \mu\mathrm{m}$ and $\langle P \rangle = 104{,}800\ \mathrm{Pa}$. Measurements by van der Schaaf et al. (1998) in a riser ($\omega_f^{exp} = 400$ Hz and $\omega^{exp} < 10$ Hz). C_h in $\mathrm{s}^{-1/2}$.

4.2. Filtered models

4.2.1. Effective drag coefficient approach for the filtered drag force

Fig. 3 shows the effect of an effective drag coefficient approach for the filtered drag force (Eq. (20)) on the mixture speed of sound $c_m(\omega, \varepsilon_s)$ (Eqs. (38)–(40)) calculated via a linear wave propagation speed analysis of the filtered gas–solid flow model (Eqs. (15)–(18)). As mentioned in the paragraph on *Modeling*, the effective drag models of Yang et al. (2003) and Heynderickx et al. (2004) predict a reduction of the drag coefficient β_e by a factor 1.5 to 4. With decreasing filter frequency ω_f, the effective drag coefficient β_e is, however, expected to decrease further. In particular this may be the case if the apparent added mass (Eq. (21)) (Zhang and Vander-Heyden, 2002; De Wilde, 2005b) becomes important, as discussed in the next paragraph. Therefore, and to illustrate more clearly the effect of an effective drag coefficient approach and in particular which frequencies are affected by such an approach, the mixture speed of sound behavior for a further decreasing effective drag coefficient β_e is also illustrated in Fig. 3.

As expected from the preliminary analysis of Eq. (38), an effective drag coefficient approach for the filtered drag force (Eq. (20)) affects the mixture speed of sound $c_m(\omega, \varepsilon_s)$ (Eqs. (38)–(40)) over the entire wave frequency range ω, independent of the applied effective drag coefficient. In particular, the mixture speed of sound $c_m(\omega, \varepsilon_s)$ at low wave frequencies ω is also altered as soon as the drag coefficient is reduced. Furthermore, as the effective drag coefficient β_e decreases, the high frequency mixture speed of sound is gradually introduced to lower wave frequencies. Fig. 2a ($\beta_e = \beta/10$, $C_a = 0$) quantitatively illustrates that using the effective drag coefficient approach for the filtered drag force (Eq. (20)), the filtered gas–solid flow model (Eqs. (15)–(18)) over predicts the experimentally observed low frequency limit mixture speed of sound. Hence, such a filtered model cannot be expected to accurately describe the low frequency, i.e. filtered, gas–solid flow field.

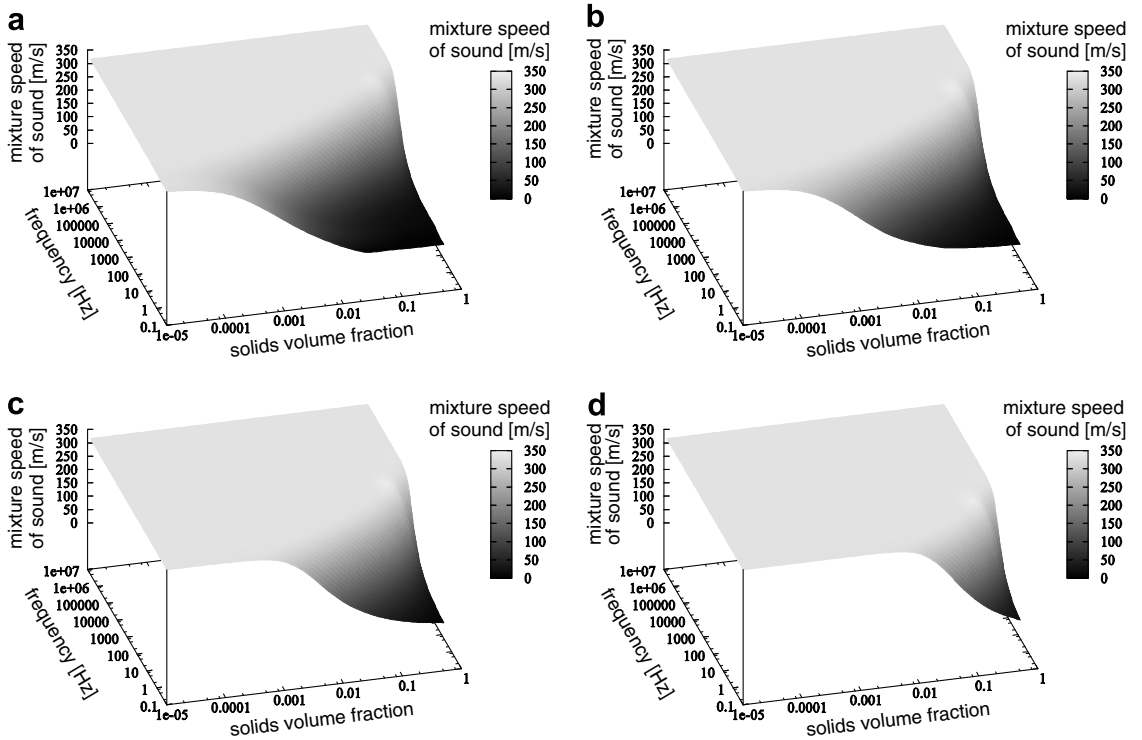

Fig. 3. Mixture speed of sound c_m (Eqs. (38)–(40)) as a function of the angular wave frequency and the solids volume fraction calculated from a linear wave propagation speed analysis of the filtered model (Eqs. (15)–(18), (20)) with: (a) effective drag coefficient β_e of Heynderickx et al. (2004), (b) $\beta_e = \beta/10$, (c) $\beta_e = \beta/100$ and (d) $\beta_e = \beta/1000$. Conditions: $\rho_s = 2650$ kg m^{-3}, $\rho_g = 0.934$ kg m^{-3}, d_p=310 μm and $\langle P \rangle = 104{,}800$ Pa. (a) → (d): $\beta_e \downarrow$ as $\omega_f \downarrow$.

4.2.2. Apparent added mass approach for the correlation between the solids volume fraction and the gas phase pressure gradient

Fig. 4 shows the effect of an apparent added mass approach for the correlation between the solids volume fraction and the gas phase pressure gradient $\left\langle \varepsilon_s' \frac{\partial P'}{\partial \mathbf{r}} \right\rangle$ (Eq. (21)) on the behavior of the mixture speed of sound $c_m(\omega, \varepsilon_s)$ (Eqs. (38)–(40)) calculated via a linear wave propagation speed analysis of the filtered model (Eqs. (15)–(18)). According to Eq. (21), as the filter frequency ω_f decreases and $\left\langle \varepsilon_s' \frac{\partial P'}{\partial \mathbf{r}} \right\rangle$ grows in importance, the apparent added mass coefficient C_a is expected to increase. Fig. 4 shows that, as the apparent added mass coefficient C_a increases, the mixture speed of sound $c_m(\omega, \varepsilon_s)$ is progressively altered from the high wave frequencies ω on. According to its definition, the filter frequency ω_f resulting from using the filtered apparent added mass based model can be derived from Fig. 4 as the frequency up to which the mixture speed of sound $c_m(\omega, \varepsilon_s)$ is not altered and remains being calculated correctly, that is in agreement with the non-filtered model (Fig. 1). Figs. 1 and 4 demonstrate that, using an apparent added mass approach, it is in fact the filter frequency mixture speed of sound $c_m(\omega_f, \varepsilon_s)$ that is introduced to wave frequencies ω higher than the filter frequency ω_f. It should be stressed that the mixture speed of sound $c_m(\omega, \varepsilon_s)$ for wave frequencies ω lower than the filter frequency ω_f is not altered and remains being predicted correctly by the filtered model. Hence, as the filter frequency ω_f decreases and the apparent added mass coefficient C_a increases, the low frequency limit mixture speed of sound behavior is progressively introduced over the entire frequency range. An added mass type description not affecting the entire frequency range is in agreement with the preliminary analysis of Eq. (38).

It should be emphasized that the impact of the apparent added mass closure term (Eq. (21)) on the mixture speed of sound $c_m(\omega, \varepsilon_s)$ calculated from the filtered model (Eqs. (15)–(18)) is in agreement with the behavior generally expected from filtered models. As the filter frequency ω_f decreases, the filtered model progressively destroys its capability of predicting the mixture speed of sound $c_m(\omega, \varepsilon_s)$ for wave frequencies ω higher than the filter frequency ω_f, while keeping its capability of predicting the mixture speed of sound $c_m(\omega, \varepsilon_s)$ for wave frequencies ω lower than the filter frequency ω_f (Fig. 4).

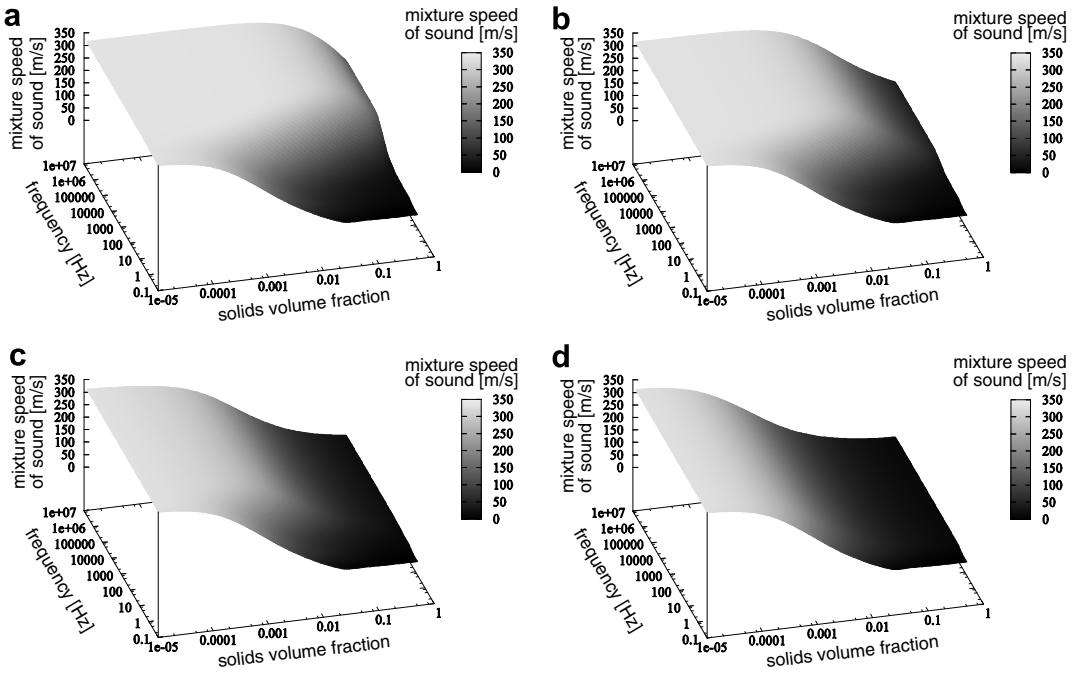

Fig. 4. Mixture speed of sound c_m (Eqs. (38)–(40)) as a function of the angular wave frequency and the solids volume fraction calculated from a linear wave propagation speed analysis of the filtered model Eqs. (15)–(18), (20) and (21) with an effective drag coefficient β_e (Heynderickx et al., 2004) and with an apparent added mass (Zhang and VanderHeyden, 2002) with: (a) $C_a = 0.002$, (b) $C_a = 0.02$, (c) $C_a = 0.2$,(d) $C_a = 2$. Conditions: $\rho_s = 2650\ \mathrm{kg\ m^{-3}}$, $\rho_g = 0.934\ \mathrm{kg\ m^{-3}}$, $d_p = 310\ \mu\mathrm{m}$ and $\langle P \rangle = 104{,}800\ \mathrm{Pa}$. (a) → (d): $C_a\uparrow$ as $\omega_f\downarrow$.

Fig. 5 presents, for two solid phase densities ρ_s of respectively 250 and 2650 kg m^{-3}, estimates of the maximum allowable apparent added mass coefficient C_a (Eq. (21)) (Zhang and VanderHeyden, 2002) as a function of the filter frequency ω_f, determined from an evaluation of the mixture speed of sound behavior $c_m(\omega, \varepsilon_s)$ (Eqs. (38)–(40)) of the filtered model (Eqs. (15)–(18)) with an apparent added mass closure for the correlation between the solids volume fraction and the gas phase pressure gradient (Eq. (21)). As mentioned before, for a given apparent added mass coefficient C_a, the corresponding filter frequency ω_f is obtained by comparing the filtered mixture speed of sound behavior for that value of C_a (Fig. 4) with the non-filtered mixture speed of sound behavior (Fig. 1). An arbitrary limit of 2% is imposed on the difference in the mixture speed of sounds. For example, with a solids density ρ_s of 2650 kg m^{-3}, for an apparent added mass coefficient C_a of 0.002, the mixture speed of sound $c_m(\omega, \varepsilon_s)$ for wave frequencies ω lower than about 200 Hz is accurately predicted, whereas for an apparent added mass coefficient C_a of 0.02, only the mixture speed of sound $c_m(\omega, \varepsilon_s)$ for wave frequencies lower than about 40 Hz is accurately predicted. As the solids density ρ_s decreases, the maximum allowable apparent added mass coefficient C_a for a given filter frequency ω_f increases (Fig. 5). Figs. 4 and 5 furthermore demonstrate that apparent added mass coefficient values larger than 1, as stated by Zhang and VanderHeyden (2002), are indeed possible and allowable for filter frequencies ω_f lower than 10 Hz. Such low filter frequencies are unlikely to be introduced by spatial filtering, as this would imply mesh dimensions of the order of meters, but are easily introduced by temporal filtering, as for example in steady state simulations.

For low filter frequencies ω_f, the apparent added mass closure (Eq. (21)) is able to restore the limit low frequency mixture speed of sound behavior $c_m(\varepsilon_s)$ of the filtered model (Eqs. (15)–(18)), eventually altered by making use of an effective drag approach (Eq. (20)) (see previous paragraph). The impact of the apparent added mass on the low-frequency limit mixture speed of sound $c_m(\varepsilon_s)$ is quantitatively illustrated in Fig. 2a for the effective drag coefficient β_e of Heynderickx et al. (2004) ($\frac{\beta}{4} < \beta_e < \frac{2\beta}{3}$), for an effective drag coefficient $\beta_e = \beta/10$ and for the limiting case of an effective drag coefficient β_e going to zero. In any effective drag coefficient case, quite large apparent added mass coefficients C_a are required to accurately restore the low-frequency limit mixture speed of sound behavior $c_m(\varepsilon_s)$. Interestingly, as the filter frequency ω_f decreases and the value of β_e decreases, the value of C_a required to accurately restore the low-frequency limit mixture speed of sound behavior increases, as it should. For values of C_a larger than 1, any higher frequency or frequency dependent mixture speed of sound behavior is destroyed (Fig. 4). In fact, with such large values of C_a, the effective drag coefficient β_e may become very small, as discussed further in this paper. At intermediate filter frequencies ω_f, the impact of an effective drag coefficient β_e (Eq. (20)) on the mixture speed of sound $c_m(\omega, \varepsilon_s)$ at wave frequencies ω lower than the filter frequency ω_f (Fig. 3) can, however, not fully, that is over the entire non-filtered frequency range, be compensated for by the apparent added mass. Hence, the effective drag coefficient concept (Eq. (20)) and its combination with an apparent added mass (Eq. (21)) is to be investigated further.

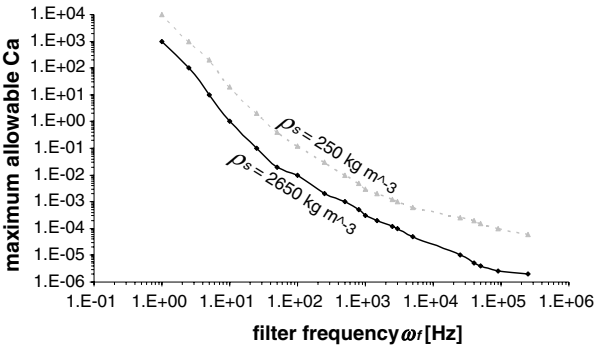

Fig. 5. Maximum allowable apparent added mass coefficient C_a (Eq. (21)) as a function of the filter frequency ω_f. Determined from a linear wave propagation speed analysis with the filtered model (Eqs. (15)–(18) and (21)) with drag and with an apparent added mass (Zhang and VanderHeyden, 2002). Conditions: $\rho_s = 250$ or 2650 kg m^{-3}, $\rho_g = 0.934$ kg m^{-3}, $d_p = 310$ μm and $\langle P \rangle = 104{,}800$ Pa.

Fig. 6 illustrates that the apparent added mass closure for the correlation between the solids volume fraction and the gas phase pressure gradient (Eq. (21)) does not introduce any intrinsic frequency dependence in the mixture speed of sound c_m (Eqs. (38)–(40)). This is in agreement with the lack of any frequency dependence in the mixture speed of sound c_m being introduced by the momentum transfer source term $\varepsilon_s(\partial P/\partial \mathbf{r})$ in the non-filtered model (Eqs. (1)–(6)). Hence, if an apparent added mass approach (Eq. (21)) is taken and if a frequency dependence in the mixture speed of sound c_m is required, that is for intermediate filter frequencies ω_f, it must be provided by a drag or effective drag term (Fig. 4).

Somehow, the effect of filtering the drag force (Eq. (20)) and the effect of the correlation between the solids volume fraction and the gas phase pressure gradient (Eq. (21)) are related. As the filter frequency ω_f decreases and the effective drag coefficient β_e (Eq. (20)) decreases, the correlation between the solids volume fraction and the gas phase pressure gradient $\left\langle \varepsilon_s' \frac{\partial P'}{\partial \mathbf{r}} \right\rangle$ (Eq. (21)) becomes more important. A possible explanation is that, as the filter frequency ω_f decreases, the microscopic description of the gas–solid momentum transfer provided by the drag force (Eqs. (3), (5) and (20)) is progressively replaced by a more macroscopic description provided by the apparent added mass (Eq. (21)). The latter is better understood by reformulating the apparent added mass as an apparent distribution of the filtered gas phase pressure gradient over the phases and an apparent (effective) drag force. As will be shown in what follows, the apparent added mass contribution to the filtered description of the gas–solid momentum transfer introduces itself a reduction of the (effective) drag force contribution and, hence, introduces an apparent (effective) drag force (to be distinguished from the effective drag force introduced in Eq. (20)). The reformulation of the apparent added mass was explained by De Wilde (2005b). The presence of the drag force was, however, neglected in the analysis. Accounting for the presence of the drag force, it can analytically and in a way similar to De Wilde (2005b) be shown that:

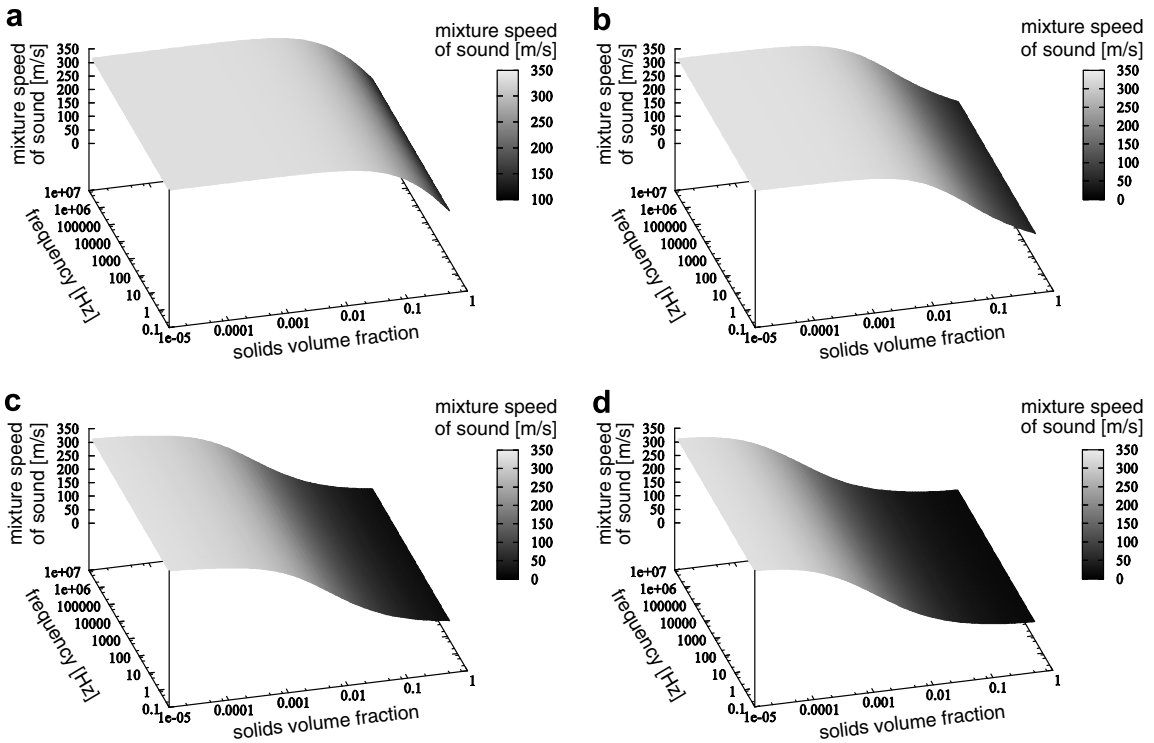

Fig. 6. Mixture speed of sound c_m (Eqs. (38)–(40)) as a function of the angular wave frequency and the solids volume fraction calculated from a linear wave propagation speed analysis of the filtered model (Eqs. (15)–(18), (21)) without drag and with an apparent added mass (Zhang and VanderHeyden, 2002) with: (a) $C_a = 0.002$, (b) $C_a = 0.02$, (c) $C_a = 0.2$ and (d) $C_a = 2$. Conditions: $\rho_s = 2650\ \mathrm{kg\ m^{-3}}$, $\rho_g = 0.934\ \mathrm{kg\ m^{-3}}$, $d_p = 310\ \mu\mathrm{m}$ and $\langle P \rangle = 104{,}800\ \mathrm{Pa}$. (a) → (d): $C_a\uparrow$ as $\omega_f\downarrow$.

$$C_a\langle\rho_m\rangle\left(\frac{\partial\{\mathbf{v}\}}{\partial t}+\{\mathbf{v}\}\cdot\frac{\partial\{\mathbf{v}\}}{\partial\mathbf{r}}-\frac{\partial\{\mathbf{u}\}}{\partial t}-\{\mathbf{u}\}\cdot\frac{\partial\{\mathbf{u}\}}{\partial\mathbf{r}}\right)$$
$$=\frac{C_a\langle\varepsilon_g\rangle\langle m_s\rangle}{\left(\frac{\langle\varepsilon_s\rangle\langle\varepsilon_g\rangle\rho_s\rho_g}{\langle\rho_m\rangle^2}\right)+C_a}\left\langle\frac{\partial P}{\partial\mathbf{r}}\right\rangle+\frac{C_a}{\left(\frac{\langle\varepsilon_s\rangle\langle\varepsilon_g\rangle\rho_s\rho_g}{\langle\rho_m\rangle^2}\right)+C_a}\langle\beta(\mathbf{u}-\mathbf{v})\rangle \tag{47}$$

with $\langle m_s\rangle$ the Reynolds-averaged solids mass fraction:

$$\langle m_s\rangle=\frac{\langle\varepsilon_s\rangle\rho_s}{\langle\varepsilon_s\rangle\rho_s+\langle\varepsilon_g\rangle\rho_g} \tag{48}$$

and combining Eqs. (19), (21) and (47), the filtered gas–solid momentum transfer, i.e. the combination of the filtered momentum transfer term $\langle\varepsilon_s(\partial P/\partial\mathbf{r})\rangle$ and the filtered drag force $\langle\beta(\mathbf{u}-\mathbf{v})\rangle$ in Eqs. (17) and (18), can be written as

$$\left\langle\varepsilon_s\frac{\partial P}{\partial\mathbf{r}}\right\rangle-\langle\beta(\mathbf{u}-\mathbf{v})\rangle=\left(\langle\varepsilon_s\rangle+\frac{C_a\langle\varepsilon_g\rangle\langle m_s\rangle}{\left(\frac{\langle\varepsilon_s\rangle\langle\varepsilon_g\rangle\rho_s\rho_g}{\langle\rho_m\rangle^2}\right)+C_a}\right)\left\langle\frac{\partial P}{\partial\mathbf{r}}\right\rangle+\left[\frac{C_a}{\left(\frac{\langle\varepsilon_s\rangle\langle\varepsilon_g\rangle\rho_s\rho_g}{\langle\rho_m\rangle^2}\right)+C_a}-1\right]\langle\beta(\mathbf{u}-\mathbf{v})\rangle \tag{49}$$

A more general description of the distribution factor of the filtered gas phase pressure gradient over the solid phase in terms of the mean square of the solids volume fraction fluctuations, avoiding the introduction of the apparent added mass coefficient C_a, was derived by De Wilde (2005b). An apparent (effective) drag force is seen to result from pre-multiplying the filtered drag force – modelled as an effective drag force according to Eq. (20) – with an apparent added mass related prefactor.

Using Eqs. (20) and (49), the filtered solid phase and gas phase momentum equations (Eqs. (17) and (18)) can be rewritten as

Filtered momentum conservation solid phase:

$$\frac{\partial}{\partial t}(\langle\varepsilon_s\rangle\rho_s\{\mathbf{v}\})+\frac{\partial}{\partial\mathbf{r}}\cdot(\langle\varepsilon_s\rangle\rho_s\{\mathbf{v}\}\{\mathbf{v}\})=-\frac{\partial}{\partial\mathbf{r}}\langle P_s\rangle-\frac{\partial}{\partial\mathbf{r}}\cdot(\langle\varepsilon_s\rangle\{\tilde{\mathbf{s}}_s\})+\langle\varepsilon_s\rangle\rho_s\mathbf{g}$$
$$-\left(\langle\varepsilon_s\rangle+\frac{C_a\langle\varepsilon_g\rangle\langle m_s\rangle}{\left(\frac{\langle\varepsilon_s\rangle\langle\varepsilon_g\rangle\rho_s\rho_g}{\langle\rho_m\rangle^2}\right)+C_a}\right)\left\langle\frac{\partial P}{\partial\mathbf{r}}\right\rangle$$
$$+\left[1-\frac{C_a}{\left(\frac{\langle\varepsilon_s\rangle\langle\varepsilon_g\rangle\rho_s\rho_g}{\langle\rho_m\rangle^2}\right)+C_a}\right]\beta_e(\{\mathbf{u}\}-\{\mathbf{v}\}) \tag{50}$$

Filtered momentum conservation gas phase:

$$\frac{\partial}{\partial t}(\langle\varepsilon_g\rangle\rho_g\{\mathbf{u}\})+\frac{\partial}{\partial\mathbf{r}}\cdot(\langle\varepsilon_g\rangle\rho_g\{\mathbf{u}\}\{\mathbf{u}\})=-\left\langle\frac{\partial P}{\partial\mathbf{r}}\right\rangle-\frac{\partial}{\partial\mathbf{r}}\cdot\langle\tilde{\mathbf{s}}_g\rangle+\langle\varepsilon_g\rangle\rho_g\mathbf{g}$$
$$+\left(\langle\varepsilon_s\rangle+\frac{C_a\langle\varepsilon_g\rangle\langle m_s\rangle}{\left(\frac{\langle\varepsilon_s\rangle\langle\varepsilon_g\rangle\rho_s\rho_g}{\langle\rho_m\rangle^2}\right)+C_a}\right)\left\langle\frac{\partial P}{\partial\mathbf{r}}\right\rangle$$
$$-\left[1-\frac{C_a}{\left(\frac{\langle\varepsilon_s\rangle\langle\varepsilon_g\rangle\rho_s\rho_g}{\langle\rho_m\rangle^2}\right)+C_a}\right]\beta_e(\{\mathbf{u}\}-\{\mathbf{v}\}) \tag{51}$$

For very high filter frequencies ω_f, the apparent added mass coefficient C_a approaches zero (Fig. 5) and the effective drag coefficient β_e (Eq. (20)) approaches the non-filtered drag coefficient β, Eq. (49) logically reducing to:

$$\left\langle \varepsilon_s \frac{\partial P}{\partial \mathbf{r}} \right\rangle - \langle \beta(\mathbf{u}-\mathbf{v}) \rangle = \langle \varepsilon_s \rangle \left\langle \frac{\partial P}{\partial \mathbf{r}} \right\rangle - \beta(\{\mathbf{u}\} - \{\mathbf{v}\}) \tag{52}$$

Hence, for very high filter frequencies ω_f, the non-filtered gas–solid momentum transfer model is retrieved, as it should.

For the limit of very low filter frequencies ω_f (e.g. steady state calculations), on the other hand, the apparent added mass coefficient C_a may become large (Zhang and VanderHeyden, 2002; De Wilde, 2005; Fig. 5). Rewriting the apparent added mass related prefactor of the filtered drag force as $\left[\frac{1}{1+\left(\frac{\langle \varepsilon_s \rangle \langle \varepsilon_g \rangle \rho_s \rho_g}{C_a \langle \rho_m \rangle^2}\right)} - 1\right]$, it is easily seen that for large values of the apparent added mass coefficient C_a Eq. (49) reduces to:

$$\begin{aligned} \left\langle \varepsilon_s \tfrac{\partial P}{\partial \mathbf{r}} \right\rangle - \langle \beta(\mathbf{u}-\mathbf{v}) \rangle &= (\langle \varepsilon_s \rangle + \langle \varepsilon_g \rangle \langle m_s \rangle) \left\langle \tfrac{\partial P}{\partial \mathbf{r}} \right\rangle + [1-1]\beta_e(\{\mathbf{u}\} - \{\mathbf{v}\}) \\ &= (\langle m_s \rangle + \langle \varepsilon_s \rangle (1 - \langle m_s \rangle)) \left\langle \tfrac{\partial P}{\partial \mathbf{r}} \right\rangle \\ &\approx \langle m_s \rangle \left\langle \tfrac{\partial P}{\partial \mathbf{r}} \right\rangle \end{aligned} \tag{53}$$

In the low filter frequency limit filtered description of gas–solid momentum transfer, a mass fraction based distribution of the filtered gas phase pressure gradient over the phases is obtained and the effective drag contribution to the filtered description of gas–solid momentum transfer vanishes, Eqs. (50) and (51) reducing to:

$$\frac{\partial}{\partial t} \langle \varepsilon_s \rangle \rho_s \{\mathbf{v}\} + \frac{\partial}{\partial \mathbf{r}} \cdot (\langle \varepsilon_s \rangle \rho_s \{\mathbf{v}\}\{\mathbf{v}\}) = -\frac{\partial}{\partial \mathbf{r}} \langle P_s \rangle - \frac{\partial}{\partial \mathbf{r}} \cdot (\langle \varepsilon_s \rangle \{\tilde{\mathbf{s}}_s\}) + \langle \varepsilon_s \rangle \rho_s \mathbf{g} - \langle m_s \rangle \left\langle \frac{\partial P}{\partial \mathbf{r}} \right\rangle \tag{54}$$

and

$$\frac{\partial}{\partial t} (\langle \varepsilon_g \rangle \rho_g \{\mathbf{u}\}) + \frac{\partial}{\partial \mathbf{r}} \cdot (\langle \varepsilon_g \rangle \rho_g \{\mathbf{u}\}\{\mathbf{u}\}) = -\left\langle \frac{\partial P}{\partial \mathbf{r}} \right\rangle - \frac{\partial}{\partial \mathbf{r}} \cdot \langle \tilde{\mathbf{s}}_g \rangle + \langle \varepsilon_g \rangle \rho_g \mathbf{g} + \langle m_s \rangle \left\langle \frac{\partial P}{\partial \mathbf{r}} \right\rangle \tag{55}$$

The effective drag contribution to the filtered gas–solid momentum transfer description vanishing with a mass fraction based distribution of the filtered gas phase pressure gradient over the phases, limits the solid phase acceleration by gas–solid momentum transfer to the gas phase acceleration. Eqs. (20) and (49) teach that, as the filter frequency ω_f decreases, the microscopic drag force type description of the gas–solid momentum transfer is progressively replaced by a more macroscopic description that basically consists of distributing the filtered gas phase pressure gradient, the ultimate macroscopic driving force of both the phases, over the phases. Summarizing, whereas with very high filter frequencies ω_f the drag force type description of gas–solid momentum transfer is applicable, with very low filter frequencies ω_f an apparent distribution of the filtered gas phase pressure gradient over the phases (e.g. Eq. (53)) and, hence, an apparent added mass type description (Eq. (21)) makes sense. However, as discussed before, at intermediate filter frequencies ω_f, a combination of an effective drag approach (Eq. (20)) and an apparent added mass approach (Eq. (21)) may not always give an adequate filtered description of gas–solid momentum transfer, a more complex approach being needed. The apparent added mass approach introducing an acceptable behavior for filtered gas–solid momentum transfer models (Fig. 4), its reformulation (Eq. (47)) suggests that a redistribution or effective distribution of the filtered gas phase pressure gradient over the phases may compensate for the unacceptable behavior introduced by an effective drag approach (Eq. (20)) (Fig. 3).

It should be remarked that the mixture momentum model (Gidaspow, 1994) exhibits the same mixture speed of sound behavior $c_m(\varepsilon_s)$ as the low filter frequency limit filtered model Eqs. (54) and (55), i.e. with a high value of the apparent added mass coefficient C_a (Fig. 4d), but whereas the low filter frequency limit

filtered model Eqs. (54) and (55) allows slip between the phases, the mixture momentum model assumes equal phase velocities, excluding slip between the phases.

4.2.3. Apparent history force approach for the correlation between the solids volume fraction and the gas phase pressure gradient

Fig. 7 shows the mixture speed of sound $c_m(\omega, \varepsilon_s)$ calculated via a linear wave propagation speed analysis of the filtered model (Eqs. (15)–(18)) using an apparent history force closure model for the correlation between the solids volume fraction and the gas phase pressure gradient $\left\langle \varepsilon_s' \frac{\partial P'}{\partial r} \right\rangle$ (Eq. (22)). As the filter frequency ω_f decreases, $\left\langle \varepsilon_s' \frac{\partial P'}{\partial r} \right\rangle$ grows in importance and the value of the apparent history force coefficient C_h is expected to increase. No values for the apparent history force coefficient C_h are reported in literature so far, but, referring to the possible relation with the inverse of the square root of the time scale of the solids clusters, values much larger than 1 $s^{-1/2}$ are possible.

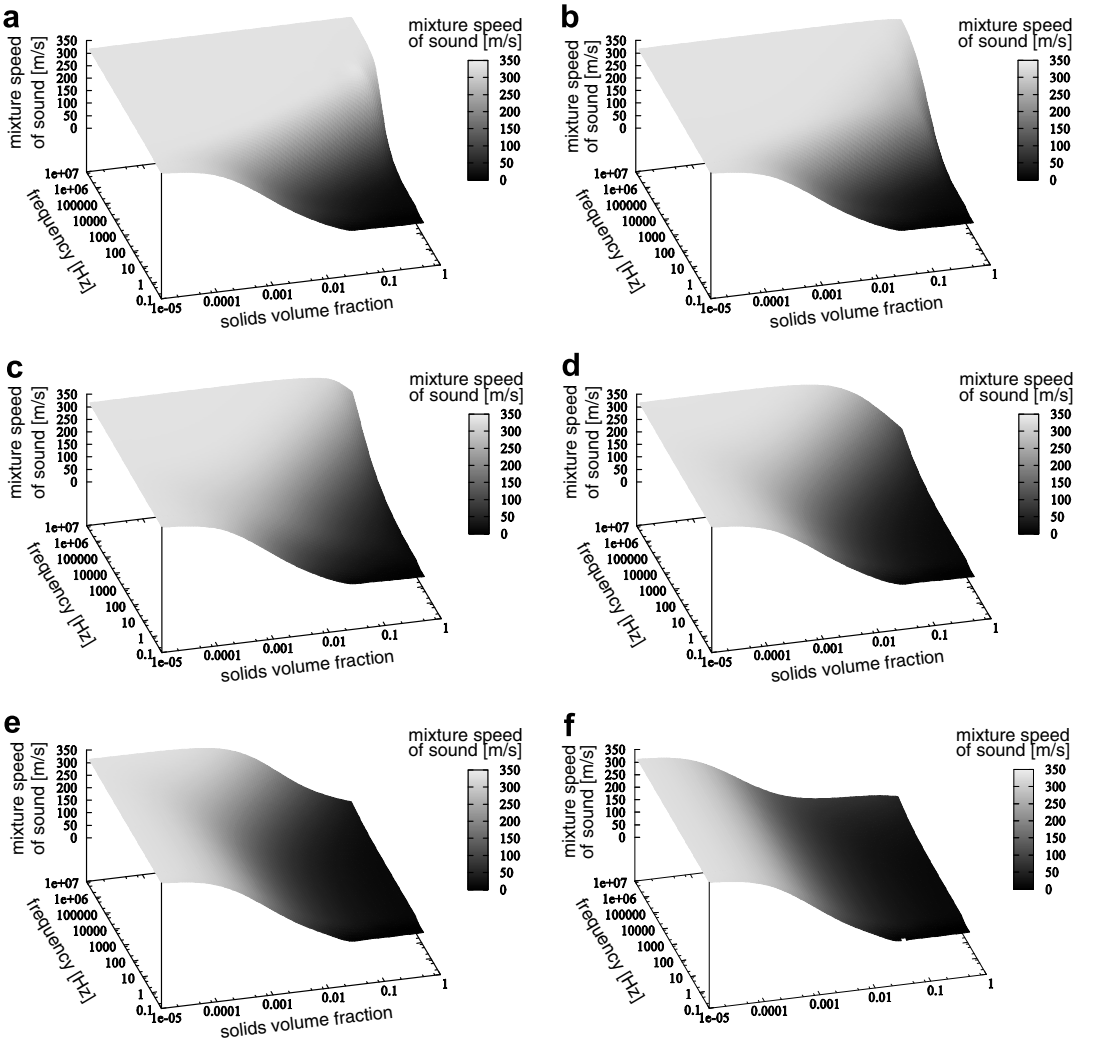

Fig. 7. Mixture speed of sound c_m (Eqs. (38)–(40)) as a function of the angular wave frequency and the solids volume fraction calculated from a linear wave propagation speed analysis of the filtered model (Eqs. (15)–(18), (20) and (22)) with an effective drag coefficient β_e (Heynderickx et al., 2004) and with an apparent history force with: (a) $C_h = 0.2\ s^{-1/2}$, (b) $C_h = 2\ s^{-1/2}$, (c) $C_h = 20\ s^{-1/2}$, (d) $C_h = 200\ s^{-1/2}$, (e) $C_h = 2000\ s^{-1/2}$ and (f) $C_h = 20000\ s^{-1/2}$. Conditions: $\rho_s = 2650\ kg\ m^{-3}$, $\rho_g = 0.934\ kg\ m^{-3}$, $d_p = 310\ \mu m$ and $\langle P \rangle = 104{,}800$ Pa. (a) → (f): $C_h\uparrow$ as $\omega_f\downarrow$.

An initial increase of the apparent history force coefficient C_h hardly affects the calculated mixture speed of sound $c_m(\omega, \varepsilon_s)$ (Fig. 7). As the apparent history force coefficient C_h increases further, the low frequency mixture speed of sound behavior is progressively introduced over all frequencies, but from the high solids volume fractions and the low frequencies on. The latter is undesirable for a filtered model. This becomes more clear from Fig. 8, showing the intrinsic effects introduced by the apparent history force (Eq. (22)) in the mixture speed of sound $c_m(\omega, \varepsilon_s)$ calculated from the filtered model (Eqs. (15)–(18)), i.e. in the absence of a drag force. In contrast with the apparent added mass (Eq. (21)) (Fig. 6) and as expected from the preliminary analysis of Eq. (38), an apparent history force introduces an intrinsic frequency dependence of the mixture speed of sound, except for very large values of the apparent history force coefficient $C_h(C_h \approx 20{,}000\ \mathrm{s}^{-1/2})$. Such a frequency dependence of the mixture speed of sound c_m intrinsic to (the closure model for) the correlation between the solids volume fraction and the gas phase pressure gradient is not expected from the momentum transfer source term $\varepsilon_s(\partial P/\partial \mathbf{r})$ in the non-filtered model (Eqs. (1)–(6)).

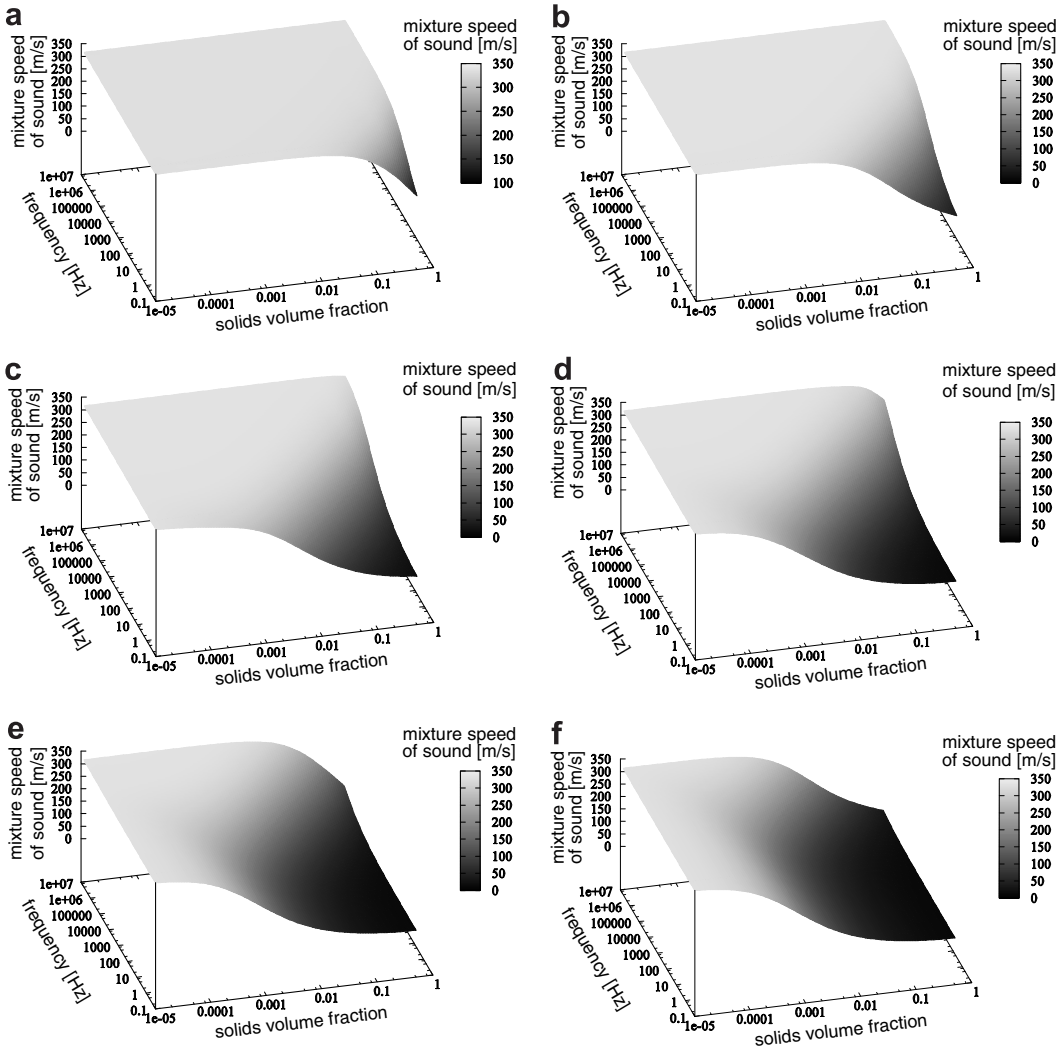

Fig. 8. Mixture speed of sound c_m (Eqs. (38)–(40)) as a function of the angular wave frequency and the solids volume fraction calculated from a linear wave propagation speed analysis of the filtered model (Eqs. (15)–(18), (20) and (22)) without drag and with an apparent history force with: (a) $C_h = 0.02\ \mathrm{s}^{-1/2}$, (b) $C_h = 0.2\ \mathrm{s}^{-1/2}$, (c) $C_h = 2\ \mathrm{s}^{-1/2}$, (d) $C_h = 20\ \mathrm{s}^{-1/2}$, (e) $C_h = 200\ \mathrm{s}^{-1/2}$ and (f) $C_h = 2000\ \mathrm{s}^{-1/2}$. Conditions: $\rho_s = 2650\ \mathrm{kg\ m}^{-3}$, $\rho_g = 0.934\ \mathrm{kg\ m}^{-3}$, $d_p = 310\ \mu\mathrm{m}$ and $\langle P \rangle = 104{,}800\ \mathrm{Pa}$. (a) → (f): $C_h\uparrow$ as $\omega_r\downarrow$.

Analogous to the apparent added mass (Eq. (21)), the apparent history force (Eq. (22)) is capable of restoring the low frequency limit mixture speed of sound behavior, eventually altered by taking an effective drag coefficient approach for the filtered drag force (Eq. (20)) (Fig. 3). A quantitative comparison of the experimentally measured low frequency limit mixture speed of sound $c_m(\varepsilon_s)$ (van der Schaaf et al., 1998) with the low frequency limit mixture speed of sound $c_m(\varepsilon_s)$ calculated using an apparent history force (Eq. (22)) in the absence of drag (Fig. 2b), shows that an accurate calculation of the low frequency limit mixture speed of sound $c_m(\varepsilon_s)$ is still possible, but requires large values of the apparent history force coefficient ($C_h > 200\ s^{-1/2}$). In such case, any higher frequency or frequency dependent behavior of the mixture speed of sound c_m is destroyed (Fig. 7).

The behavior originating from the apparent history force closure for the correlation between the solids volume fraction and the gas phase pressure gradient (Eq. (22)) (Fig. 8) is interesting in the sense that via the apparent history force, the filtered momentum transfer term $\langle \varepsilon_s(\partial P/\partial \mathbf{r})\rangle$ may, at least qualitatively, introduce the wave frequency and solids volume fraction dependent mixture speed of sound behavior $c_m(\omega, \varepsilon_s)$ (Atkinson and Kytömaa, 1992; Gregor and Rumpf, 1975, 1976; van der Schaaf et al., 1998) generally attributed to the presence of the drag force (Gregor and Rumpf, 1975, 1976) (Fig. 1). The apparent history force explanation for the mixture speed of sound behavior suggests, however, that a certain filter frequency ω_f is required to observe a frequency and solids volume fraction dependence of the mixture speed of sound c_m. With respect to the latter, it is important to recognize that experimental observations indeed also suffer from a filter frequency ω_f^{exp}. The experimental filter frequency ω_f^{exp} of the low frequency ($\omega^{exp} < 10$ Hz) mixture speed of sound measurements by van der Schaaf et al. (1998) (Fig. 2), for example, was about 400 Hz.

As a closure model for the correlation between the solids volume fraction and the gas phase pressure gradient (Eq. (22)), an apparent history force seems, however, not suited, the mixture speed of sound $c_m(\omega, \varepsilon_s)$ being altered from the low wave frequencies ω on. Therefore, according to the linear wave propagation speed test proposed in this paper, an apparent added mass (Eq. (21)) (Zhang and VanderHeyden, 2002; De Wilde, 2005) is so far the only promising closure model approach for the correlation between the solids volume fraction and the gas phase pressure gradient $\left\langle \varepsilon_s' \frac{\partial P'}{\partial \mathbf{r}} \right\rangle$.

5. Conclusions

The wave frequency dependence of the linear wave propagation speeds in gas–solid flows is related to gas–solid momentum transfer and allows a simple test for filtered gas–solid momentum transfer models. The linear wave propagation speeds obtained from filtered models are compared with those obtained from the non-filtered model. Whereas filtered models may alter the linear wave propagation speeds at wave frequencies higher than the filter frequency, filtered models may not alter the linear wave propagation speeds at wave frequencies lower than the filter frequency.

An effective drag coefficient closure model approach for the filtered drag force, proposed by Yang et al. (2003), Heynderickx et al. (2004) and Andrews et al. (2005), is observed to alter the linear wave propagation speeds over the entire wave frequency range, independent of the applied effective drag coefficient. As the effective drag coefficient decreases, the high frequency linear wave propagation speed behavior is gradually introduced to lower wave frequencies. As such, the impact of an effective drag coefficient approach on the linear wave propagation speeds is undesirable for filtered models.

An apparent added mass closure model for the correlation between the solids volume fraction and the gas phase pressure gradient, proposed by Zhang and VanderHeyden (2002), introduces the desirable behavior for filtered models with respect to the linear wave propagation speeds. For a given filter frequency and corresponding apparent added mass coefficient, the linear wave propagation speeds at wave frequencies higher than the filter frequency are altered and become equal to the filter frequency linear wave propagation speeds. The linear wave propagation speeds at wave frequencies lower than the filter frequency are, however, not altered and remain to be predicted correctly, that is as with the non-filtered model. Furthermore, an apparent added mass introduces no intrinsic frequency dependence in the linear wave propagation speeds, as expected from its non-filtered source term. Hence, a frequency dependence of the linear wave propagation speeds at frequencies lower than the filter frequency is, somehow, to be provided by an effective drag force term. An apparent added mass can, however, only to a certain extent restore the linear wave propagation speed behavior at wave

frequencies lower than the filter frequency altered by an effective drag coefficient approach. An apparent added mass can be reformulated in terms of an apparent distribution of the filtered gas phase pressure gradient over the phases and an apparent (effective) drag force. As the filter frequency decreases and the apparent added mass coefficient increases, the contribution of the apparent distribution of the filtered gas phase pressure gradient over the phases to the filtered description of gas–solid momentum transfer grows in importance, whereas the contribution of the apparent (effective) drag force becomes less important.

An apparent history force closure model for the correlation between the solids volume fraction and the gas phase pressure gradient is shown to alter the linear wave propagation speeds from the low frequencies on. This is undesirable for filtered models. Furthermore, the apparent history force introduces intrinsic frequency dependence in the linear wave propagation speeds, in contrast to what is expected from its non-filtered source term.

Summarizing, whereas with very high filter frequencies the drag force type description of gas–solid momentum transfer is applicable, with very low filter frequencies the apparent added mass type description seems justified. At intermediate filter frequencies, however, a combination of these two approaches is to be further investigated and a more complex approach may be needed.

Acknowledgements

One of the authors (JDW) would like to thank S. Sundaresan of Princeton University for his interest in this work and the helpful discussions.

Two of the authors (DC and GJH) acknowledge financial support by the ''Bijzonder Onderzoeksfonds'' of the Ghent University under the GOA project ''Mackie''.

References

Agrawal, K., Loezos, P.N., Syamlal, M., Sundaresan, S., 2001. The role of meso-scale structures in rapid gas–solid flows. J. Fluid Mech. 445, 151–185.

Anderson, T., Jackson, R., 1967. A fluid mechanical description of fluidized beds. Ind. Eng. Chem. Fundam. 6, 527–539.

Andrews, A.T., Loezos, P.N., Sundaresan, S., 2005. Coarse-grid simulations of gas-particle flows in vertical risers. Ind. Eng. Chem. Res. 44, 6022–6037.

Arai, M., 1980. Characteristics and stability analyses for two-phase flow equation systems with viscous terms. Nucl. Sci. Eng. 74, 77–83.

Atkinson, C.M., Kytömaa, H.K., 1992. Acoustic-wave speed and attenuation in suspensions. Int. J. Multiphase Flow 18, 577–592.

Basset, A.B., 1961. A treatise in hydrodynamics II. Bell and Co.

Boure, J.A., 1997a. Wave phenomena and one-dimensional two-phase flow models. Part I: Kinematic waves; experimental results; theory. Multiphase Sci. Technol. 9, 1–35.

Boure, J.A., 1997b. Wave phenomena and one-dimensional two-phase flow models. Part III: General case; general drift flux models; other two-fluid models. Multiphase Sci. Technol. 9, 63–107.

Bracewell, R.N., 1965. The Fourier Transform and its Applications. McGraw Hill, New York.

Crowe, C., Sommerfeld, M., Tsuji, Y., 1997. Multiphase Flows with Droplets and Particles, first ed. CRC Press.

De Wilde, J., 2005b. Reformulating and quantifying the generalized added mass in filtered gas–solid flow models. Phys. Fluids 17, 113304.

De Wilde, J., Heynderickx, G.J., Vierendeels, J., Dick, E., Marin, G.B., 2002. An Extension of the Preconditioned Advection Upstream Splitting Method for 3D Two-Phase Flow Calculations in Circulating Fluidized Beds. Comput. Chem. Eng. 26, 1677–1702.

De Wilde, J., Vierendeels, J., Heynderickx, G.J., Marin, G.B., 2005a. Simultaneous solution algorithms for Eulerian–Eulerian gas–solid flow models: stability analysis and convergence behaviour of a point and a plane solver. J. Comput. Phys. 207, 309–353.

De Wilde, J., Baudrez, E., Heynderickx, G.J., Marin, G.B., 2005c. Preconditioning for the simultaneous solution of gas–solid flows. American Institute of Chemical Engineers, AIChE 2005 Annual Meeting, Particle Technology Forum, Cincinnati, OH, USA, October 30–November 4, 2005.

Ergun, S., 1952. Fluid flow through packed columns. Chem. Eng. Prog. 48, 89–94.

Gidaspow, D., 1994. Multiphase Flow and Fluidization: Continuum and Kinetic Theory Descriptions. Academic Press.

Gregor, W., Rumpf, H., 1975. Velocity of sound in two-phase media. Int. J. Multiphase Flow 1, 753–769.

Gregor, W., Rumpf, H., 1976. Attenuation of sound in gas–solid suspensions. Powder Technol. 15, 43–51.

Heynderickx, G.J., Das, A.K., De Wilde, J., Marin, G.B., 2004. Effect of clustering on gas–solid drag in dilute two-phase flow. Ind. Eng. Chem. Res. 43, 4635–4646.

Jenkins, J.T., Savage, S.B., 1983. A theory for the rapid flow of identical, smooth, nearly elastic, spherical-particles. J. Fluid Mech. 130, 187–202.

Mei, R., 1993. History force on a sphere due to a step change in the free-stream velocity. Int. J. Multiphase Flow 19, 509–525.

Pope, S.B., 2000. Turbulent Flows. Cambridge University Press.

Prosperetti, A., Jones, A.V., 1987. The linear-stability of general 2-phase flow models, Part 2. Int. J. Multiphase Flow 13, 161–171.
Ranade, V.V., 2002. Computational flow modeling for chemical reactor engineering. In: Process System Engineering, vol. 5. Academic Press.
Ransom, V.H., Hicks, D.L., 1984. Hyperbolic 2-pressure models for 2-phase flow. J. Comput. Phys. 53, 124–151.
Ransom, V.H., Hicks, D.L., 1988. Hyperbolic 2-pressure models for 2-phase flow revisited. J. Comput. Phys. 75, 498–504.
Stewart, H.B., Wendroff, B., 1984. 2-phase flow—models and methods. J. Comput. Phys. 56, 363–409.
van der Schaaf, J., Schouten, J.C., van den Bleek, C.M., 1998. Origin, propagation and attenuation of pressure waves in gas–solid fluidized beds. Powder Technol. 95, 220–233.
Wen, Y.C., Yu, Y.H., 1966. Mechanics of Fluidization. Chem. Eng. Prog. Symp. Ser. 62, 100–111.
Yang, N., Wang, W., Ge, W., Li, J., 2003. CFD Simulation of concurrent-up gas–solid flow in circulating fluidized beds with structure-dependent drag coefficient. Chem. Eng. J. 96, 71–80.
Zhang, D.Z., VanderHeyden, W.B., 2002. The effects of mesoscale structures on the macroscopic momentum equations for two-phase flows. Int. J. Multiphase Flow 28, 805–822.